AGU PUBLICATIONS

JGR

Journal of Geophysical Research: Atmospheres

RESEARCH ARTICLE
10.1002/2017JD027523

**Key Points:**
- New gridded monthly soil-moisture estimates indicate that the southeast U.S. drought in fall 2016 was the second most severe since at least 1895
- The driver was low precipitation, but record-high evaporative demand also contributed. Both countered centennial trends in the region
- These conditions were caused by internal atmospheric variability and were only modestly aided, if at all, by tropical teleconnections

**Supporting Information:**
- Supporting Information S1

**Correspondence to:**
A. Park Williams,
williams@ldeo.columbia.edu

**Citation:**
Park Williams, A., Cook, B. I., Smerdon, J. E., Bishop, D. A., Seager, R., & Mankin, J. S. (2017). The 2016 southeastern U.S. drought: An extreme departure from centennial wetting and cooling. *Journal of Geophysical Research: Atmospheres*, *122*, 10,888–10,905. https://doi.org/10.1002/2017JD027523

Received 27 JUL 2017
Accepted 24 SEP 2017
Accepted article online 4 OCT 2017
Published online 26 OCT 2017



# The 2016 Southeastern U.S. Drought: An Extreme Departure From Centennial Wetting and Cooling

**A. Park Williams[1], Benjamin I. Cook[2], Jason E. Smerdon[1], Daniel A. Bishop[1,3], Richard Seager[1], and Justin S. Mankin[1,2,4]**

[1]Lamont-Doherty Earth Observatory of Columbia University, Palisades, NY, USA, [2]NASA Goddard Institute for Space Studies, New York, NY, USA, [3]Department of Earth and Environmental Sciences, Columbia University, New York, NY, USA, [4]Department of Geography, Dartmouth College, Hanover, NH, USA

**Abstract** The fall 2016 drought in the southeastern United States (SE U.S.) appeared exceptional based on its widespread impacts, but the current monitoring framework that only extends from 1979 to present does not readily facilitate evaluation of soil-moisture anomalies in a centennial context. A new method to extend monthly gridded soil-moisture estimates back to 1895 is developed, indicating that since 1895, October–November 2016 soil moisture (0–200 cm) in the SE U.S. was likely the second lowest on record, behind 1954. This severe drought developed rapidly and was brought on by low September–November precipitation and record-high September–November daily maximum temperatures (Tmax). Record-high Tmax drove record-high atmospheric moisture demand, accounting for 28% of the October–November 2016 soil-moisture anomaly. Drought and heat in fall 2016 contrasted with 20th century wetting and cooling in the region but resembled conditions more common from 1895–1956. Dynamically, the exceptional drying in fall 2016 was driven by anomalous ridging over the central United States that reduced south-southwesterly moisture transports into the SE U.S. by approximately 75%. These circulation anomalies were partly promoted by a moderate La Niña and warmth in the tropical Atlantic, but these processes accounted for very little of the SE U.S. drying in fall 2016, implying a large role for internal atmospheric variability. The extended analysis back to 1895 indicates that SE U.S. droughts as strong as the 2016 event are more likely than indicated from a shorter 60 year perspective and continued multidecadal swings in precipitation may combine with future warming to further enhance the likelihood of such events.

## 1. Introduction

The southeast United States (SE U.S.) experienced an exceptional drought in the fall of 2016. According to the United States Drought Monitor (Svoboda et al., 2002), which assesses drought severity based on a range of metrics, 92% of the area within Georgia, Alabama, Mississippi, and Tennessee was in a state of "severe drought" or worse as of 29 November 2016 (Figure 1). The event peaked in October–November (Oct-Nov) and caused hundreds of millions of dollars of losses in crop sales (USDA, 2017a), major degradation of pasture and rangeland (USDA, 2017b), reservoir shortages leading to interstate disagreements over water rights (Samuel, 2016), and widespread wildfires (NASA, 2016). Regarding wildfires specifically, satellite data indicate that the SE U.S. likely had substantially more forest area burned in 2016 than in any other year since at least 1984 (Figure 1). In Gatlinburg, Tennessee, three fires in November 2016 burned over 11,000 ha, damaging or destroying more than 2,460 structures and leading to 14 fatalities (Ahillen, 2016). Prior to 2016, other notable SE U.S. droughts occurred in 1954 (Chen et al., 2012), 1986 (Cook et al., 1988; Trenberth et al., 1988), 2000 (Klos et al., 2009), and 2007 (Seager et al., 2009). The combined effects of the 2016 drought in the SE U.S. indicate that this may have been among the most severe droughts of the past century, but direct comparison of this event to earlier droughts is not straightforward due to a lack of long-term assessments of the regional moisture balance. For instance, the U.S. Drought Monitor data only extend from the year 2000 to present, and the drought-classification methodology has varied over time. Alternative approaches are therefore necessary to assess the 2016 SE U.S. drought in a centennial context, identify the dynamics that force such droughts, and improve SE U.S. drought predictability.

For multidecade evaluations of historical drought variability, land-surface models (LSMs, e.g., Ek et al., 2003; Koster & Suarez, 1994; Wood et al., 1992) are powerful tools for assessing historical drought events, quantifying the relative contributions of various components of the water balance to these droughts, and monitoring drought severity operationally (e.g., Livneh & Hoerling, 2016). To assist with assessment of historical and

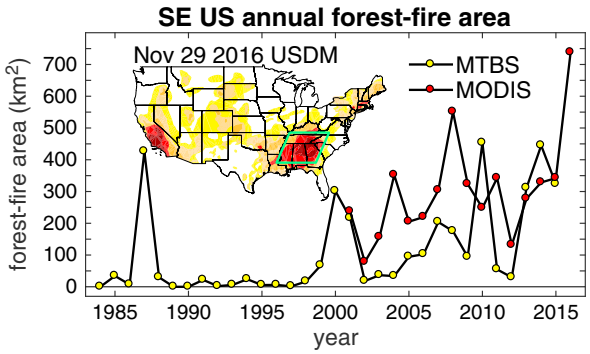


**Figure 1.** Satellite-derived annual forest-fire area in the SE U.S. from 1984–2016 according to (red dots) the version 6 burned area product from the Moderate Resolution Infrared Spectrometer (MODIS; Roy et al., 2008) and (yellow dots) the record of large (≥202 ha) fires from the U.S. Forest Service Monitoring Trends in Burn Severity product (MTBS; Eidenshink et al., 2007). MTBS records do not yet extend through 2016. Burned area is aggregated within 1/120° grid cells that are defined as having ≥75% forest cover according to the LANDFIRE Environmental Site Potential data set (www.landfire.gov). The SE U.S. region is outlined in the map inset, which also shows the U.S. Drought Monitor (USDM) drought classifications on 29 November 2016, where white, yellow, beige, orange, red, and dark red indicate no drought, abnormally dry, moderate drought, severe drought, extreme drought, and exceptional drought, respectively.

ongoing hydrological variations, the second phase of the National Land Data Assimilation (NLDAS2) provides publicly available hourly grids of outputs (including soil moisture at various depths) from three LSMs covering the period from 1979 to present across the continental U.S., northern Mexico, and southern Canada (Xia et al., 2012a; Xia et al., 2012b). NLDAS2 data are updated daily and are key considerations in the weekly drought assessments produced by the U.S. Drought Monitor.

The NLDAS2 period from 1979 to present is not ideal for capturing a comprehensive range of drought variability, however, because low-frequency (decadal to centennial) climate variations such as the Interdecadal Pacific Oscillation and the Atlantic Multidecadal Oscillation (AMO) are likely to cause hydroclimate variability that is not well represented in a given 30–40 year period (McCabe et al., 2004). For the SE U.S., the lack of NLDAS2 simulations prior to 1979 is particularly problematic because recent decades have been wet and cool relative to the early 21st century, perhaps causing the 2016 event to appear less likely than a longer perspective would suggest (Higgins et al., 2000; Pan et al., 2004; Seager et al., 2012; Wang et al., 2009). Additionally, the NLDAS2 does not include supplemental simulations necessary for the attribution of observed soil-moisture anomalies to individual components of the moisture balance (e.g., Livneh & Hoerling, 2016; Williams et al., 2015). For a longer-term perspective on historical drought variability and efficient decomposition of this variability into contributions from various drivers, bucket-type water-balance indices such as the Palmer Drought Severity Index (PDSI; Palmer, 1965) and the Standardized Precipitation-Evaporation Index (Vicente-Serrano et al., 2010) are often considered (e.g., Cook et al., 2014; Williams et al., 2015), but these metrics are less physically representative (e.g., Koster & Suarez, 1994) and some practitioners find standardized drought metrics less useful than more tangible quantifications such as soil-moisture content (e.g., Steinemann, 2014; Steinemann et al., 2015). In this paper, we investigate centennial drought variability while attempting to strike a balance between the rigor of an LSM and the efficient applicability of a bucket-type water-balance calculation.

In addition to better understanding the historical context and local causes of the recent SE U.S. drought, there is also interest in its large-scale dynamical drivers and potential links to sea surface temperature (SST) patterns relevant for hydroclimatic forecasting (e.g., Li et al., 2011; Nigam et al., 2011; Seager et al., 2009). To date, little research has been done to better understand SE U.S. hydroclimatic variability during the fall season specifically, when the 2016 drought impacts were most severe. While weeks or months with a high frequency of rain-free days are common in the western U.S., such a situation is relatively rare in the SE U.S. (e.g., Dai et al., 2007; Gershunov & Cayan, 2003) and can therefore, at any time of year, have serious consequences for dense forests, rain-fed agriculture, and shallow reservoirs that are reliant on regular precipitation. Furthermore, temperatures and solar intensity in the region are relatively high, leading to relatively high evaporative demand throughout the year. The serious consequences of the SE U.S. drought in fall 2016 therefore incentivize deeper understanding of the drought's evolution, historical context, and causes.

In this study, we improve our understanding of the fall 2016 drought in the SE U.S. in terms of its long-term context and dynamical drivers. We first establish a novel approach to use gridded monthly climate data sets to reliably derive estimates of soil-moisture anomalies simulated by a complex LSM back to 1895. The established record of estimated soil moisture then allows us to address the following questions:

1. Relative to 1979–2016, how do LSMs characterize 2016 soil-moisture anomalies in terms of location, severity, and timing of the SE U.S. drought?
2. In a centennial context, how anomalous were the SE U.S. surface-climate conditions that caused the 2016 drought and how did they relate to previously established trends?
3. What was the centennial context of 2016 soil-moisture anomalies and what were the roles of precipitation and evaporation?

4. What were the dynamical drivers of the drought and were these drivers associated with well-known modes of global climate variability?

## 2. Data and Methods

### 2.1. Study Region

We define the SE U.S. study region as the green polygon shown in Figure 1; the geographic coordinates of the four corners of the region are (northwest) 37°N, 89°W; (northeast) 37°N, 80°W; (southeast) 31°N, 83°W; and (southwest) 31°N, 92°W. The region excludes the area of anomalous moisture associated with Hurricane Matthew in early October 2016 and broadly bounds the zone of anomalous drought in fall 2016 based on the NLDAS2 modeled soil moisture described below.

### 2.2. Modeled Soil Moisture

Hourly modeled soil moisture gridded at 1/8° geographic resolution for 1979–2016 come from the NLDAS2 (Xia et al., 2012b) Noah LSM (Ek et al., 2003; Niu et al., 2011). Analyses reported in this paper are for soil moisture within the 0–200 cm soil column. The 0–200 cm layer extends to the deepest model layer, most comprehensively representing the soil-moisture balance of the region. Hereinafter, Noah 0–200 cm soil moisture is referred to as $SM_{Noah}$. For each grid cell, daily and monthly relative $SM_{Noah}$ anomalies (fraction of the mean) are expressed relative to the 1979–2016 mean annual cycle of daily values.

### 2.3. Surface-Climate Data for 1895 to Present

We use records of precipitation and reference evapotranspiration (ETo, also commonly referred to as potential evapotranspiration) gridded at 1/8° geographic resolution for January 1895 through June 2017. We calculate ETo using the physically based Penman-Monteith formula (Monteith, 1965) following Allen et al. (1998), which requires monthly means of daily maximum temperature (Tmax), daily minimum temperature (Tmin), vapor pressure, 2 m wind speed, and solar radiation at the surface. Data on precipitation, Tmax, and Tmin for the continental U.S. are from the National Oceanic and Atmospheric Administration Climgrid data set (Vose et al., 2014). Vapor pressure is calculated from PRISM gridded dew-point data (Daly et al., 2008). Climgrid and PRISM have 1/24° geographic resolution that we aggregate to the NLDAS2 resolution of 1/8°. For wind velocity and solar radiation, we use a combination of the 1/8° resolution NLDAS2 meteorological forcing and the 1/2° Princeton Global Forcing version 2 (Sheffield et al., 2006), bilinearly downscaled to 1/8° resolution and rescaled temporally to match the mean climatology of NLDAS2 during overlapping years. Notably, there are a range of gridded climate data products available for the U.S. Our chosen climate data sets are generally within the range of variability among data sets for the SE U.S. region, particularly for precipitation and Tmax, which are the primary drivers of interannual drought variability (Figure S1 in the supporting information; Compo et al., 2011; Daly et al., 2008; Harris et al., 2014; Oyler et al., 2015; Rodell et al., 2004; Rohde et al., 2013; Schneider et al., 2014). Additional details about the surface-climate data sets are available in Text S1 and Table S1 in the supporting information.

We evaluate climate trends using the nonparametric Theil-Sen estimator (Sen, 1968), which is more robust to outliers than linear regression. Trend significance is considered at the $p < 0.05$ level according to the Kendall's Tau test and following adjustment for reductions in effective sample size due to first-order autocorrelation.

### 2.4. Centennial Soil-Moisture Estimates

The relatively short NLDAS2 record inhibits characterization of soil-moisture anomalies in a long-term (centennial) context. To assess variations in the soil-moisture balance from 1895 to present, we estimate records of monthly mean soil moisture at 1/8° geographic resolution based on monthly gridded records of precipitation and ETo. These estimates are based on a new monthly Model Calibrated Drought Index (MCDI) that we introduce here, which reliably replicates the soil-moisture outputs from the Noah LSM that is traditionally forced by high-frequency (30 min) meteorological data. The ability to reliably estimate LSM soil moisture from monthly climate data is an advance that allows us to temporally extend our evaluation of SE U.S. drought for periods that are beyond the NLDAS2 record and for which high-frequency meteorological data sets are limited while saving on computational costs. The basis of the MCDI is a relatively simple bucket model, but for each grid cell, the monthly persistence of the MCDI is tuned to reflect the monthly persistence characteristics of 0–200 cm soil-moisture anomalies from the more complex Noah LSM. This

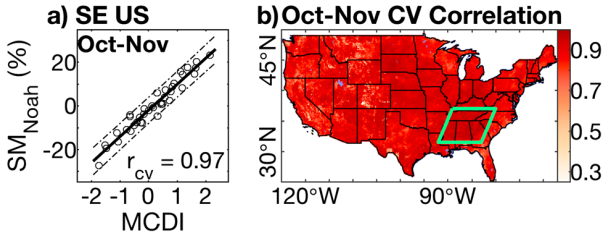


**Figure 2.** Cross-validated (CV) correlation between 0–200 cm modeled soil moisture ($SM_{Noah}$) anomalies and the model calibrated drought index (MCDI) during Oct-Nov for (a) the SE U.S. region and (b) across the continental U.S. The dotted lines in Figure 2a bound the 95% cross-validated confidence intervals for sample prediction. Correlation coefficients indicate the cross-validated Pearson's correlation ($r_{cv}$). The green polygon in Figure 2b bounds the SE U.S. study region. The blue areas indicate lakes and coastal regions within the continental U.S. for which there are no $SM_{Noah}$ records. MCDI was calculated from NLDAS2 climate data.

marks an important advance beyond the traditional bucket-model approach to moisture-balance accounting (e.g., Williams et al., 2015) because the Noah LSM accounts for complexities such as geographically varying soil compositions (affecting drainage rate and storage capacity), geographically and temporally varying vegetation types (affecting evapotranspiration rates), storage of above- and below-ground moisture in frozen form (affecting seasonality of infiltration, evapotranspiration, and runoff), and moisture exchange between near-surface soil and the underlying aquifer (affecting drainage rate) (Niu et al., 2011). Here we describe the methodology behind the MCDI and demonstrate its ability to use monthly gridded precipitation and ETo to reliably estimate monthly soil-moisture records generated by the more complex Noah LSM across much of the continental U.S., including all of the SE U.S.

The basis of the MCDI is the Palmer *Z*-index, which is a standardized record of monthly changes in the near-surface moisture balance based on a simple 2-layer bucket model, where monthly inputs are deposited via precipitation and monthly withdrawals are a function of ETo and the fraction of available moisture (Palmer, 1965; Text S2 for more details). From the *Z*-index, we calculated monthly MCDI as a linear combination of prior month MCDI and current month *Z*-index:

$$\text{MCDI}_m = P(\text{MCDI}_{m-1}) + (1 - P)(Z\text{-index}_m), \quad (1)$$

where $P$ is a persistence term between 0 and 1, describing the influence of prior-month (subscript $m - 1$) soil-moisture anomalies on current month (subscript $m$) soil-moisture anomalies.

This is similar to the PDSI framework, but in the PDSI algorithm $P$ is constant throughout the year and across space (0.73). In contrast to this traditional PDSI approach, we derive $P$ directly from the Noah model for each grid cell and month, allowing $P$ to vary seasonally and geographically. Seasonal and geographic variations in $P$ are reasonable because the persistence of soil moisture is dependent on the seasonality of climate (e.g., spring soil-moisture anomalies persist through summer in locations with little summer precipitation) and geographic variation in soil type and vegetation cover (e.g., soil-moisture anomalies may be less persistent in shallow soils or densely vegetated forests with high evapotranspiration rates). For each grid cell, and for each of the 12 months, we determined $P$ empirically by finding the value between 0.005 and 0.995 (in steps of 0.005) that optimizes the interannual correlation between MCDI and $SM_{Noah}$ anomalies when the MCDI calculation is forced by NLDAS2 climate data.

The optimal mean monthly persistence (averaged for the 12 months) for the SE U.S. is 0.51 (95% of grid cells: 0.33–0.64), indicating substantially less persistence in the Noah model than is assumed in the PDSI calculation. This monthly persistence varies seasonally, reaching an annual minimum in spring (regionally averaged persistence: 0.39 in March to May) and an annual maximum in fall (regionally averaged persistence is 0.63 in October to December) (Figure S2a). Low monthly persistence in spring indicates that modeled soil moisture correlates strongly with concurrent precipitation (Figure S2b). Precipitation in the SE U.S. has low monthly autocorrelation and peaks in spring, often leading to soil saturation (as evidenced by an annual peak in modeled daily aboveground runoff), diminishing the impacts of antecedent conditions. Higher monthly persistence occurs in fall when precipitation totals are lower and soil moisture is more heavily influenced by precipitation from antecedent months.

Spatially, persistence strongly varies across the continental U.S. and throughout the SE U.S. (Figures S2c and S2d). Among SE U.S. grid cells, mean monthly persistence is dictated more by soil characteristics than by climate, where areas with more permeable, well-drained soils experience less persistent soil-moisture anomalies. This interpretation is supported by a strong spatial correlation ($r = -0.91$) between annually averaged persistence values and the fraction of total precipitation that is lost through belowground runoff (Figures S2c and S2d).

For each grid cell and each of the 12 months, the MCDI values derived from NLDAS2 climate were linearly regressed against $SM_{Noah}$ anomalies (Figure S3); the regression parameters were saved for later estimation

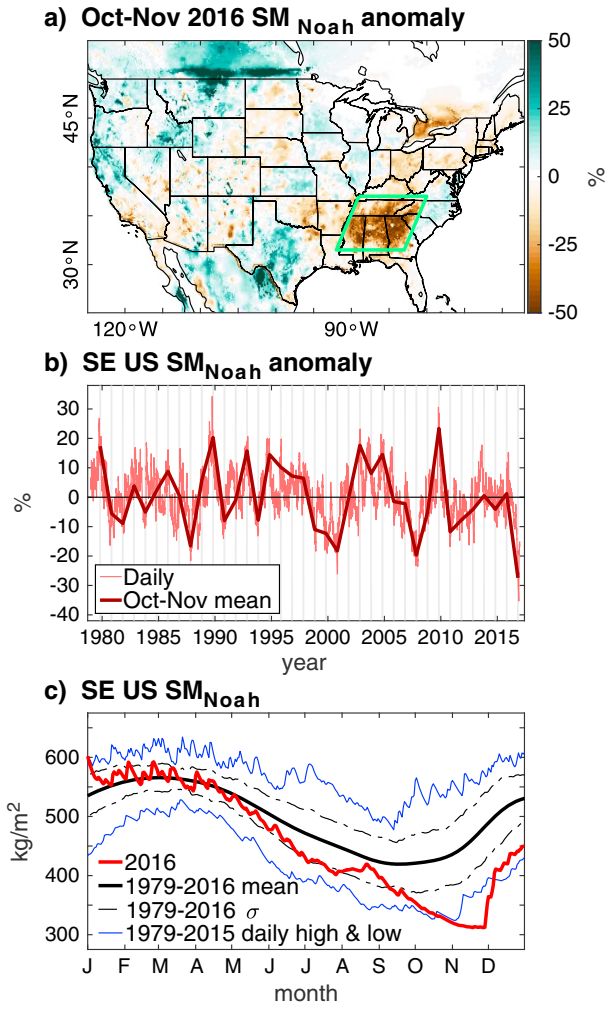


**Figure 3.** Noah modeled 0–200 cm soil moisture ($SM_{Noah}$): 1979–2016. (a) Oct-Nov 2016 $SM_{Noah}$ anomalies relative to the 1979–2016 mean. Green polygon: Southeast U.S. (SE U.S.) study region. (b) Daily and Oct-Nov relative $SM_{Noah}$ anomalies. The vertical shaded lines indicate Oct-Nov periods and the year ticks on the *x* axis represent 1 January. (c) Deviation of 2016 daily $SM_{Noah}$ (red) from the mean 1979–2016 annual cycle (thick black). Dashed black lines: one standard deviation ($\sigma$) from the mean. Blue lines: 1979–2015 record high and low values.

of soil-moisture anomalies based on MCDI calculated from non-NLDAS2 climate data. To test the utility of MCDI as a proxy for $SM_{Noah}$, we performed "leave-one-out" cross validation (Michaelsen, 1987) for the entire parameterization process: for each year we recalculated cross-validated monthly persistence parameters based all other years, recalculated MCDI records from these cross-validated persistence parameters, and calculated new estimations of $SM_{Noah}$ based on the cross-validated MCDI values.

Based on cross validation, modeled variations in monthly $SM_{Noah}$ in the SE U.S. can be reliably estimated from variations in MCDI. Cross-validated correlations between regionally averaged SE U.S. $SM_{Noah}$ anomalies and MCDI are particularly strong in summer and fall (Figure S3) and reach 0.97 for Oct-Nov (Figure 2a). Cross-validated correlations for Oct-Nov are also high at the grid-cell level throughout the SE U.S. (mean: 0.93). Beyond the SE U.S., cross-validated correlations are high throughout the continental U.S. (mean: 0.89), allowing for comparison of soil-moisture conditions in the SE U.S. to those outside that region (Figure 2b). Cross-validated correlations are also strong across much of the U.S. in other seasons, with the lowest performance occurring in seasons and regions when and where snowmelt dynamics are important (Figure S4). Strong cross-validated correlation confirms the utility of the MCDI to extend Oct-Nov $SM_{Noah}$ anomalies prior to the NLDAS2 period based on the linear relationships between these variables. To distinguish from $SM_{Noah}$, we refer to our MCDI-based estimates of soil moisture as $SM_{MCDI}$. Notably, 20th century increases in the density of the SE U.S. weather-station network could affect the temporal variability of regionally averaged $SM_{MCDI}$, but we find no trends in the spatial variability of SE U.S. $SM_{MCDI}$ to support this.

To better understand the relative influences of precipitation versus ETo in driving SE U.S. drought variability, we decomposed $SM_{MCDI}$ anomalies into contributions from precipitation versus ETo. The contribution of precipitation is determined by recalculating MCDI and $SM_{MCDI}$ anomalies for an idealized case in which only precipitation varies and ETo is held at 1921–2000 climatology. The contribution of ETo is then the difference between the original $SM_{MCDI}$ estimates and $SM_{MCDI}$ recalculated only based on precipitation variability (e.g., Williams et al., 2015). This approach requires that $SM_{MCDI}$ anomalies driven by ETo are linearly additive to those driven by precipitation. Indeed, $SM_{MCDI}$ in the SE U.S. responds as expected when ETo anomalies are artificially reduced to 25%, 50%, and 75% of observed (Figure S5).

### 2.5. Climate Dynamics Analysis

To investigate the large-scale climate processes driving SE U.S. hydroclimatic variability, we used the National Aeronautical and Space Agency (NASA) second phase of the Modern Era Retrospective Analysis for Research (MERRA-2) reanalysis data set for 1980–2016 (Molod et al., 2015; Rienecker et al., 2011). For maps of geopotential height anomalies, geopotential heights were adjusted to remove positive trends associated with the mean global warming trend during the MERRA-2 record and resultant thermal expansion of the atmosphere (Li et al., 2011; Text S3 for details).

## 3. Results

### 3.1. Relative to 1979–2016, How Do LSMs Characterize 2016 Soil-Moisture Anomalies in Terms of Location, Severity, and Timing of the SE U.S. Drought?

The $SM_{Noah}$ record indicates strong soil drying during summer and fall 2016 throughout much of the SE U.S., reaching a minimum in late November (Figure 3). Mean Oct-Nov $SM_{Noah}$ in 2016 was below the 1979–2016 average across all of the SE U.S. and was driest on record across 50% of the region (Figure 3a). Averaged

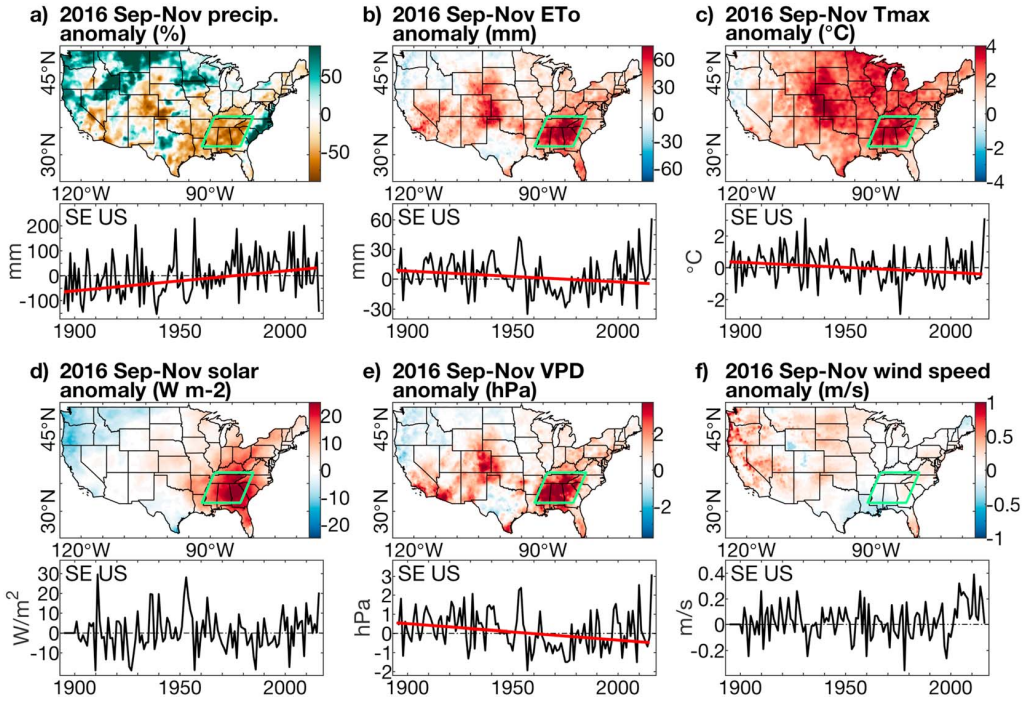


**Figure 4.** Observed Sep-Nov climate anomalies relative to 1921–2000 means. (maps) 2016 anomalies. Green polygons: SE U.S. study region. (time series plots) Anomalies within the SE U.S. (a) Relative anomalies (% of mean) in the map and absolute anomalies in the time series. The red lines indicate significant Theil-Sen trends for 1895–2015.

across the SE U.S., the mean Oct-Nov $SM_{Noah}$ in 2016 was the lowest on record (over the NLDAS2 interval), 27.5% (−2.32 $\sigma$) below the 1979–2016 mean. On a daily basis, SE U.S. mean $SM_{Noah}$ broke daily records in 2016 for all 31 days from 31 October to 30 Nov (Figures 3b and 3c). The second most severe drought in the $SM_{Noah}$ record peaked in fall 2007 with mean Oct-Nov $SM_{Noah}$ 19.7% below the 1979–2016 mean.

The year 2016 was also exceptional in terms of timing and rate of drying. $SM_{Noah}$ in the SE U.S. usually increases in November as evaporative demand declines, but 2016 $SM_{Noah}$ reached its annual minimum on 27 November, the latest annual minimum on record and 57 days later than the 1979–2015 median (Figure 3c). Furthermore, the record low $SM_{Noah}$ in late November 2016 came only 98 days after being near normal (2.4% below average) on 22 August and less than 11 months after achieving record-high daily values on 1 and 2 January (Figure 3c).

### 3.2. In a Centennial Context, How Abnormal Were the SE U.S. Surface-Climate Conditions That Caused the 2016 Drought and How Did They Relate to Previously Established Trends?

In Figure 4 we evaluate surface-climate variability in the SE U.S. from 1895–2016. With more temporal coverage than was possible from NLDAS2 data, anomalies are now reported with respect to long-term mean conditions during a baseline period of 1921–2000, which was also the calibration interval in our calculation of the Palmer *Z*-index (Text S2). Additionally, Figure 4 focuses specifically on September–November (Sep-Nov) because this was the period of extreme drying that culminated in record-breaking negative $SM_{Noah}$ anomalies averaged over Oct–Nov 2016 (Figure 3c). In Sep-Nov 2016, the SE U.S. regional average precipitation was 45.5% (−145 mm) below the long-term mean (Figure 4a). This was the third most negative precipitation anomaly on record; only 1939 and 1904 were lower. Prior to 2016, the last time the Sep-Nov precipitation total fell below 65% of average was in 1978.

Sep-Nov 2016 atmospheric aridity was also the highest within the 1895–2016 interval, as indicated by ETo (Figure 4b), which was 22.0% (+61 mm) above the mean, largely due to record-high mean Tmax (Figure 4c), due in part to high solar radiation (Figure 4d). The Sep-Nov 2016 Tmax anomaly was +3.10°C, slightly warmer than the second highest Tmax anomaly in 1931 (+3.09°C). The mean Tmin anomaly was less extreme

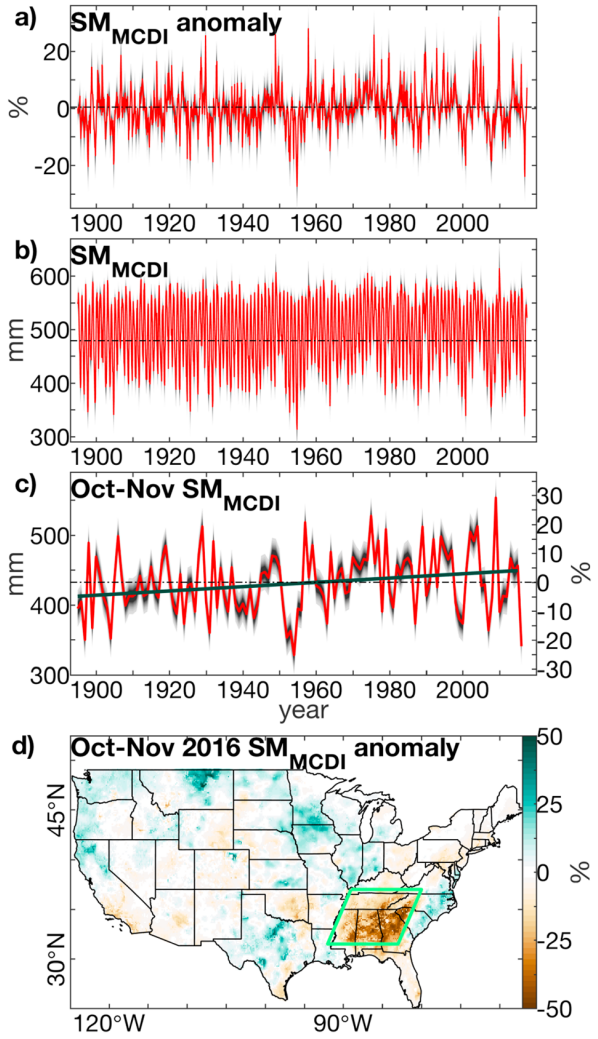


**Figure 5.** SE U.S. $SM_{MCDI}$ for January 1895 through June 2017. (a and b) Relative anomalies and absolute values, respectively. (c) Mean Oct-Nov anomalies expressed as (left axis) absolute and (right axis) relative departures from the mean. The dark green line in Figure 5c indicates the 1895–2015 trend. The shading in Figures 5a–5c bounds cross-validated 95% confidence intervals, graduating from (darker) lower to (lighter) higher confidence. (d) Map of Oct-Nov 2016 relative $SM_{MCDI}$ anomalies. Anomalies are departures from the 1921–2000 mean. The green polygon in Figure 5d bounds the SE U.S. study region.

(1.61°C above average) and was the 11th warmest on record. The warmth of Sep-Nov 2016 combined with near-normal vapor pressure to yield a record-high vapor-pressure deficit (VPD), 38.7% higher than the mean (Figure 4e). Wind speed, which multiplies the influence of VPD on ETo, was near normal (Figure 4f).

The near record-low precipitation and record-high ETo, Tmax, and VPD in Sep-Nov 2016 are particularly notable because they were in contrast to established centennial trends toward wetting and cooling in the SE U.S. (Figures 4a–4c and 4e). From 1895 to 2015, Sep-Nov precipitation increased in the region significantly ($p < 0.001$) by 47.9% (+96 mm), ETo decreased significantly ($p < 0.05$) by 4.6% (−13 mm), and Tmax decreased significantly ($p < 0.05$) by 0.77°C. The decrease in ETo was largely due to a significant ($p < 0.001$) cooling-induced decrease in VPD of 12.0%. Furthermore, although the Sep-Nov 2016 precipitation anomaly was not a record-breaking event in an absolute sense, the deviation between the observed precipitation total and that expected from trends shown in Figure 4a was by far the most negative on record.

### 3.3. What Was the Centennial Context of 2016 Soil-Moisture Anomalies and What Were the Roles of Precipitation and Evaporation?

To evaluate the centennial context of the 2016 SE U.S. drought, we use $SM_{MCDI}$ as the monthly mean soil-moisture estimate for the extended period of January 1895 through June 2017 based on the climate data sets from Figure 4 (development of the MCDI and $SM_{MCDI}$ is described in section 2.4). As with the climate data, $SM_{MCDI}$ anomalies are expressed as relative (%) departures from the 1921–2000 mean climatology. Similar to the $SM_{Noah}$ results, 2016 monthly $SM_{MCDI}$ reached its annual minima in October (relative anomaly) and November (absolute anomaly), each ranking among the lowest monthly averages over the 1895–2016 interval (Figures 5a and 5b). Considering annual Oct-Nov means, the only year with a more negative mean SE U.S. $SM_{MCDI}$ anomaly was 1954 (−26.0%; 2016: −22.9%) (Figure 5c). Accounting for uncertainties (Figure 2a), however, this is not a statistically significant difference at the 95% confidence level and there were 7 additional years when mean Oct-Nov $SM_{MCDI}$ was not significantly wetter than in 2016 (shown in Figure 6). Most of these dry fall seasons occurred in the first half of the record, however, and 2007 was the only year since 1954 with Oct-Nov $SM_{MCDI}$ comparable to that of 2016. Importantly, the near record-dry $SM_{MCDI}$ in Oct-Nov 2016 followed a significant ($p < 0.01$) positive trend (increase of 8.9%) during 1895–2015 (Figure 5c), and the 2016 anomaly marked the furthest deviation on record from this trend (as was the case for precipitation), though the 2016 $SM_{MCDI}$ departure from the trend was not significantly ($p < 0.05$) more negative than those in 1954 or 2007.

In terms of drought length, there have been several SE U.S. drought events that dwarfed the 2016 event. The longest periods without two consecutive months of above average $SM_{MCDI}$ were August 1953 through March 1957 (44 months) and November 2005 through April 2009 (42 months). By the same measure, the recent event lasted just 13 months (April 2016 through April 2017).

In terms of spatial extent across the whole of the continental U.S., the drought in Oct-Nov 2016 was much less expansive than in the other biggest drought years of the past century (Figure 6). In particular, the Oct-Nov drought conditions in 1952–1954 consumed much of the continental U.S. (Figure 6). On the other hand, Oct-Nov 2016 $SM_{MCDI}$ was lowest on record across 27.8% of the SE U.S. region (largest proportion of any

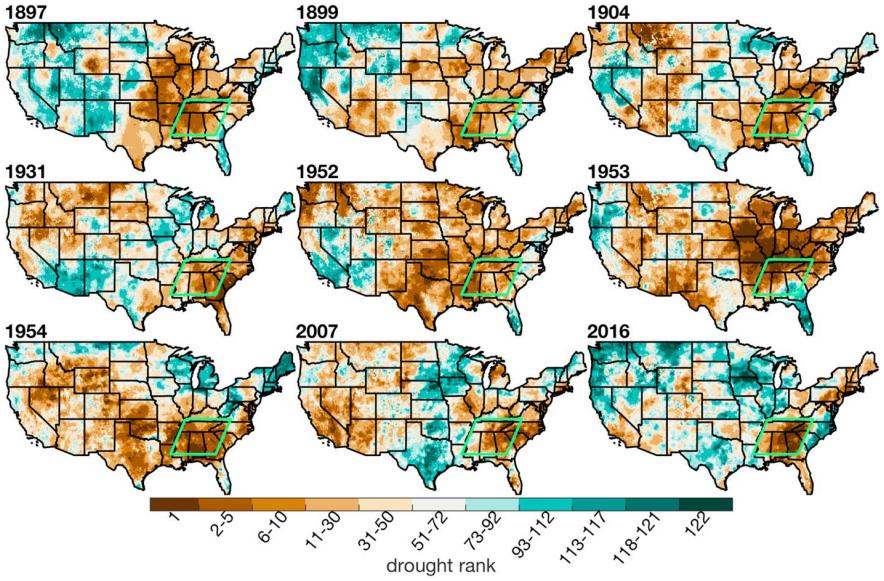


**Figure 6.** Maps of Oct-Nov drought ranking (based on $SM_{MCDI}$) for the nine driest Oct-Nov periods during 1895–2016. The lower values indicate more severe drought.

year on record), with the record-breaking drought area focused across much of the southern Appalachians, where high forest-fire forest fire activity was also concentrated in 2016. It should be noted, however, that fine-scale geographic variations in subregional hydroclimate anomalies and trends are prone to large uncertainties due to lack of station coverage and sensitivity to methodology regarding spatial interpolation of climate data (e.g., Wang et al., 2017).

Importantly, the SE U.S. region considered in this study was explicitly chosen to bound the 2016 drought area, and Oct-Nov is most extensively evaluated because this is when the 2016 drought was most intense. Comparisons of year-to-year drought severity and extent are sensitive to such choices. For example, the 1954 drought peaked in September–October and considering those months, 1954 had by far the most SE U.S. area experiencing record-low $SM_{MCDI}$ (51.5%); 2016 ranked third (6.5%) when considering the September–October window.

In comparison to other droughts, the rate at which $SM_{MCDI}$ declined in fall 2016 was particularly rapid. Similar to $SM_{Noah}$, $SM_{MCDI}$ in Oct 2016 was a record 19.5% drier than the near-normal levels in August 2016. The second most rapid relative difference between August and October $SM_{MCDI}$ occurred in 1904 (18.7%).

To contextualize the rapid SE U.S. drying in late summer and fall 2016, it is useful to compare the climatological evolution of the fall 2016 drought to other similar fall droughts. Figure 7 compares 2016 with the five other years since 1895 with the lowest mean SE U.S. Oct-Nov $SM_{MCDI}$. Among these years, all had anomalously low precipitation in all Sep-Nov months (Figure 7b) and 1904 was remarkably similar to 2016 in terms of the sequencing of monthly precipitation totals during May–December. Consequently, 1904 and 2016 followed similar $SM_{MCDI}$ trajectories throughout summer and fall. The 2 years diverge in November, when 1904 $SM_{MCDI}$ recovered slightly due, in part, to an additional 13 mm of precipitation beyond the November 2016 total.

Additionally, all years in Figure 7 experienced positive ETo anomalies throughout much of late summer and fall (Figure 7c), largely due to anomalously high VPD. In 2016, ETo was above average in all months after January, highest on record in November, and highest on record when averaged over Sep-Nov. While high ETo is to be expected in drought years due to increased solar radiation from reduced cloud cover and enhanced sensible heat flux at the expense of latent heat flux (e.g., Koster et al., 2009; Seneviratne et al., 2010; Yin et al., 2014), the record-high ETo anomaly in Sep-Nov 2016 was considerably larger than that expected based on established relationships with Sep-Nov precipitation and $SM_{MCDI}$ (Figures 7d and 7e).

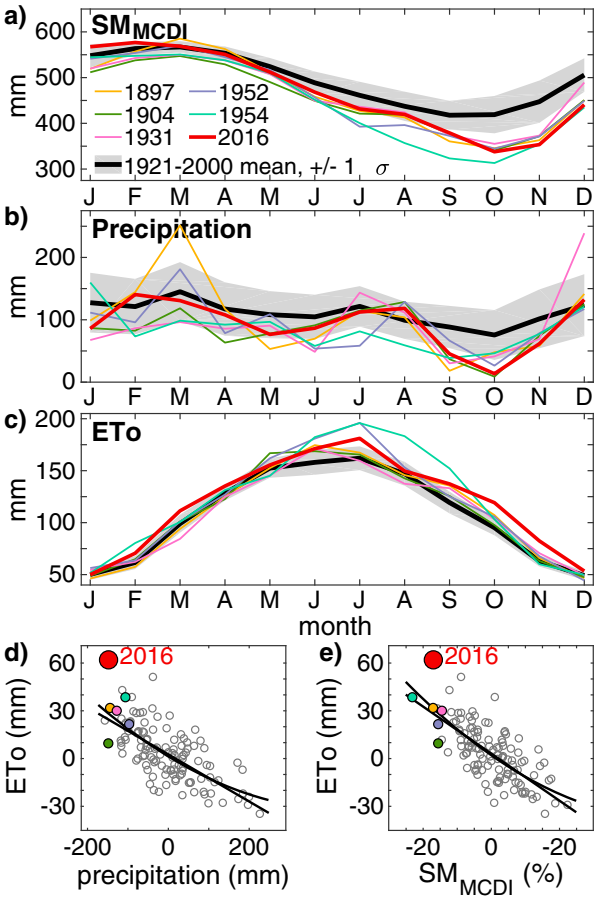


**Figure 7.** Comparison of 2016 climate to other drought years. Monthly SE U.S. (a) $SM_{MCDI}$, (b) precipitation, and (c) ETo for the 6 years with lowest Oct-Nov $SM_{MCDI}$. In Figures 7a–7c: Black bold curves and shading: 1921–2000 monthly means plus and minus one standard deviation. Scatterplots of annual Sep-Nov ETo versus (d) precipitation and (e) $SM_{MCDI}$ anomalies during the same period. The colors in Figures 7d and 7e correspond to the legend in Figure 7a. The black lines in Figures 7d and 7e represent linear and exponential regression fits, and the values in these panels are anomalies with respect to the 1921–2000 means.

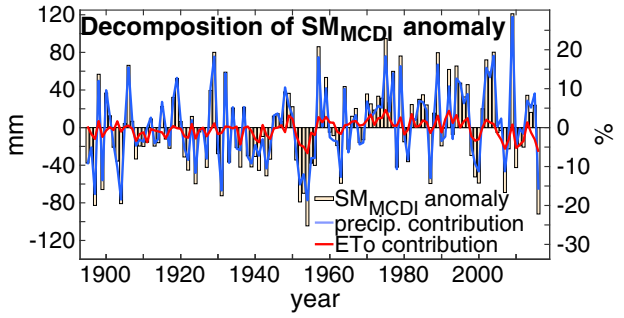


**Figure 8.** Effect of (blue) precipitation and (red) ETo on (bars) Oct-Nov SE U.S. $SM_{MCDI}$ from 1895–2016. $SM_{MCDI}$ anomalies are departures from the 1921–2000 mean and displayed in (left-hand axis) absolute and (right-hand axis) relative units.

Very high ETo values and rapid soil drying in fall 2016 motivate an evaluation of the degree to which record-high ETo enhanced the drought conditions in 2016. To estimate the effect of evaporative demand on soil moisture, we decomposed annual Oct-Nov $SM_{MCDI}$ anomalies into contributions from precipitation and ETo (Figure 8). Not including impacts of precipitation on ETo, this analysis indicates that anomalously low precipitation forced SE U.S. Oct-Nov $SM_{MCDI}$ in 2016 by −66 mm (a −16.6% deviation from the 1921–2000 mean). Anomalously high ETo negatively forced 2016 Oct-Nov $SM_{MCDI}$ by an additional −26 mm. Together, the total Oct-Nov SE U.S. $SM_{MCDI}$ anomaly is 72% attributed to low precipitation and 28% attributed to high ETo. These results were nearly identical when the analysis was repeated while only holding ETo at climatology for 2016 instead of for all years.

Over the 122 year record, declining ETo due to cooling contributed modestly to the positive $SM_{MCDI}$ trend from the early 1900s through the 1970s. Since the 1970s, however, increasing ETo due to increasing temperature, solar radiation, and wind speed have forced a negative $SM_{MCDI}$ trend beyond that caused by declining fall precipitation (Figures 4 and 8). As mentioned previously, however, ETo effects on soil moisture are not independent from precipitation effects, and this experiment's decoupling of the two processes is idealized.

### 3.4. What Were the Dynamical Drivers of the Drought and Were These Drivers Associated With Well-Known Modes of Global Climate Variability?

Here we investigate the large-scale atmosphere and ocean circulation patterns that correspond to changes in SE U.S. $SM_{MCDI}$ during fall and their roles in the extreme 2016 soil drying. To avoid detecting correlations driven by the extreme 2016 conditions, correlation analyses in this section represent 1980–2015, the period of the MERRA-2 reanalysis that excludes 2016.

Figure 9a shows the mean climatology of Sep-Nov precipitation and vertically integrated atmospheric moisture transports over North America and the surrounding areas. During fall, southwesterly winds on the western flank of the subtropical Atlantic high bring moisture to the SE U.S. from the Gulf of Mexico and southwest of North America. Southwesterly moisture transport into the SE U.S. is therefore likely an important driver of variability in Sep-Nov soil drying in the region. The correlation map in Figure 9b shows how interannual variability in Sep-Nov precipitation and moisture transports correlate with fall soil drying from 1980 to 2015; we define "fall soil drying" as the negative of the mean monthly Palmer's *Z*-index from September to November. Fall soil drying is driven largely by reductions in precipitation that are promoted by north-northeasterly circulation anomalies that suppress south-southwesterly moisture inflow from the Gulf and southwest. Sep-Nov 2016 appears as a particular case of this general fall drying configuration (Figure 9c). South-southwesterly moisture transports into the southern portion of the SE U.S. (south of 35°N) correlated significantly and negatively with Sep-Nov soil drying in 1980–2015 ($-r = 0.71$, $p < 0.001$) and were lowest on record in 2016, only 24% of the 1980–2016 average.

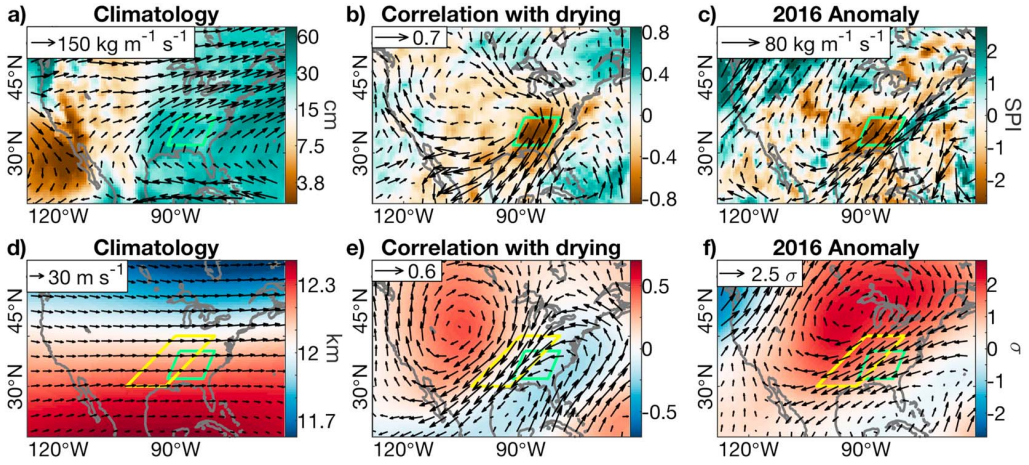


**Figure 9.** MERRA-2 Sep-Nov atmospheric circulation versus SE U.S. drying. (a–c) Precipitation and (vectors) vertically integrated moisture transports. (d–f) 200 hPa geopotential height (*Z*) and (vectors) 200 hPa wind velocity. The maps show the (Figures 9a and 9d) 1980–2016 mean climatology, (Figures 9b and 9e) correlation with Sep-Nov soil drying during 1980–2015, and (Figures 9c and 9f) the 2016 anomaly. In Figures 9b and 9c, precipitation anomalies are expressed as the Standardized Precipitation Index (SPI). The green polygon bounds the SE U.S. study region. The yellow polygon in Figures 9d–9f bounds the region where 200 hPa north-northeasterly winds correlate positively with SE U.S. drying and negatively with south-southwesterly moisture transports into the SE U.S.

For both Sep-Nov 2016 and the general case of soil drying (Figures 9b and 9c), the 200 hPa height anomaly maps indicate an upper-level anticyclonic circulation anomaly over North America and, on the east side of the anticyclone, northeasterly 200 hPa wind anomalies across much of the eastern U.S. It is these wind anomalies, and associated upper-level convergence and subsidence over the SE U.S., that inhibit southerly moisture transports into the region, moisture convergence, and precipitation. As such, for the general case of SE U.S. drying, north-northeasterly 200 hPa wind anomalies within the yellow region in Figures 9d–9f were strongly and negatively correlated with south-southwesterly moisture transports in the southern SE U.S. ($r = -0.71$, $p < 0.001$). Comparing the correlation maps in Figures 9b and 9e to the 2016 anomalies in Figures 9c and 9f, it appears that the exact position of a North American ridge can vary substantially while still suppressing moisture transports into the SE U.S. from the Gulf of Mexico.

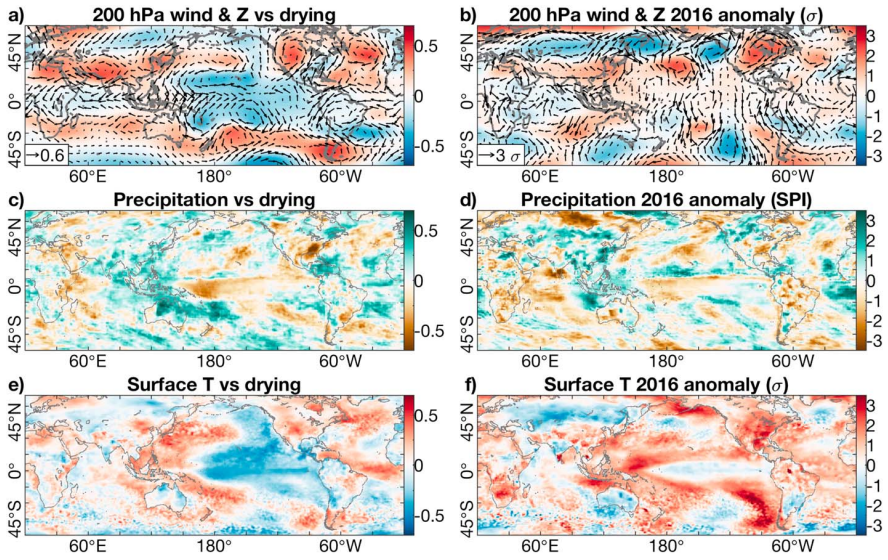


**Figure 10.** MERRA-2 global climate versus Sep-Nov drying in the SE U.S. (left) Correlation between global climate and soil drying during 1980–2015. (right) Standardized global climate anomalies in Sep-Nov 2016 relative to a 1980–2016 baseline. (top row) 200 hPa (vectors) wind velocity and (background) geopotential height (*Z*). (middle row) Precipitation, as represented by the Standardized Precipitation Index (SPI). (bottom row) Surface temperature (*T*).

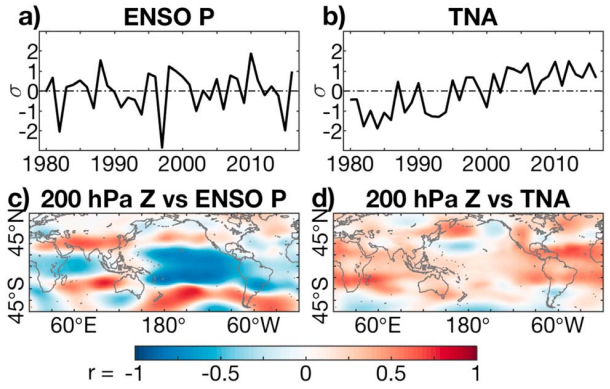


**Figure 11.** ENSO, tropical North Atlantic SSTs, and their correlations with MERRA-2 global 200 hPa geopotential height (*Z*) in Sep-Nov 1980–2015. ENSO is represented by the first principal component of tropical Sep-Nov precipitation totals (ENSO P) where positive values represent La Niña-like conditions. North Atlantic SSTs are represented by the Tropical North Atlantic (TNA) index.

We next evaluate how *global* patterns of Sep-Nov 200 hPa geopotential height and wind velocity, precipitation, and surface temperature correspond to Sep-Nov soil drying in the SE U.S. (Figure 10). For the general case, Sep-Nov drying is promoted by La Niña-like SST, precipitation, and geopotential height patterns over the tropical Pacific Ocean, indicative of the cold phase of the El Niño–Southern Oscillation (ENSO) (Figures 10a, 10c, and 10e). In the extratropics, SE U.S. drying is associated with a wave train that appears to propagate from the North Pacific across North America to the North Atlantic. It has a higher zonal wave number character that is distinct from the more canonical, larger scale, Pacific-North America wave train associated with La Niña during winter but is consistent with prior analyses of La Niña impacts in Sep-Nov (Seager et al., 2014). Additionally, the general case of SE U.S. drying is associated with warm SST anomalies in the tropical North Atlantic (Figure 10e), consistent with previous findings (Kushnir et al., 2010; Nigam et al., 2011; Ting et al., 2014; Wang et al., 2010). Indeed, the geopotential height anomalies associated with the general case of SE U.S. drying (Figure 10a) are broadly consistent over North America with those associated with a warm AMO during fall (Nigam et al., 2011). Figures 10b, 10d, and 10f indicate that during Sep-Nov 2016, SST anomalies were broadly reflective of conditions expected of La Niña in the tropical Pacific and a warm tropical North Atlantic, but the La Niña-like anomalies were less striking in 2016 than those generally associated with SE U.S. drying. Global 200 hPa height anomalies in 2016 (Figure 10b) also bore some resemblance to the pattern expected from the general drying case, albeit with differences in the specific locations of ridges and troughs in the Pacific-North America-Atlantic wave train.

To further investigate the potential forcing by ENSO and tropical North Atlantic SSTs, we relate MERRA-2 200 hPa geopotential heights globally to ENSO and the Tropical North Atlantic index (TNA; Enfield et al., 1999) for Sep-Nov 1980–2015 (Figure 11). The atmospheric component of ENSO is represented by the first principal component of Sep-Nov tropical precipitation totals (data from the Global Precipitation Climatology Project; Adler et al., 2003). We refer to this atmospheric component of ENSO as "ENSO P" and positive values represent La Niña-like conditions. Standardized time series of Sep-Nov ENSO P and TNA for 1980–2016 are shown in Figures 11a and 11b, verifying that both modes were anomalously positive (La Niña-like, warm tropical North Atlantic) in 2016, but not exceptionally so (~+1$\sigma$). The upper-tropospheric responses to ENSO P and TNA (Figures 11c and 11d) resemble the patterns associated with fall drying in the SE U.S. (Figure 10a) in terms of a northward displacement of the jet over the U.S., a ridge over central North America, and lower heights over the east coast of the U.S. and the western subtropical North Atlantic. As shown in Figure 9, these circulation anomalies would suppress southerly moisture transports to the SE U.S. from the Gulf of Mexico.

Importantly, the correlations in Figures 11c and 11d over the northern Hemisphere extratropics are relatively weak, especially over North America. Impacts on SE U.S. fall hydroclimate would therefore only be substantial when ENSO P or TNA anomalies are quite strong, which was not the case in 2016. While La Niña conditions and warm tropical North Atlantic SSTs in fall do indeed tend to correspond to reduced precipitation, higher ETo, and soil drying in the SE U.S. (Figures 12a–12f), the positive ENSO P and TNA anomalies in 2016 were simply too weak to account for a large proportion of the observed SE U.S. hydroclimate anomalies (Figures 12g–12l). It has been suggested before that a negative state of the North Pacific Oscillation may modulate the effect of La Niña on eastern U.S. precipitation (Gershunov & Barnett, 1998), but we find no such effect. To investigate the potential for SST teleconnection effects not captured by our correlation-based approach, we evaluated results of a 16-member simulation of the NCAR Community Atmospheric Model version 5.3 (CAM5.3) forced by observed SSTs for 1979–2016 (run at LDEO). The ensemble mean did not indicate an SST-forced precipitation shortfall in the SE US in Sep–Nov 2016, suggesting an even larger role for internal atmospheric variability than was suggested by our correlation-based results.

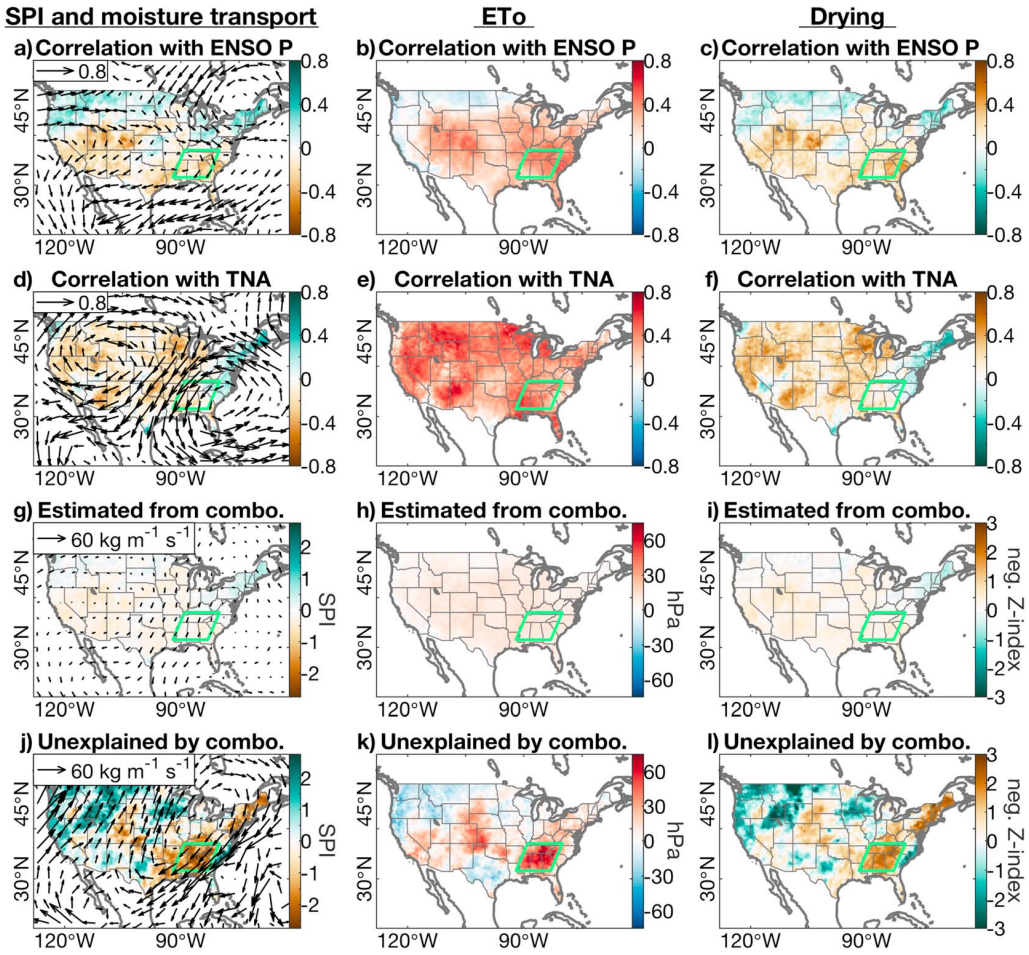


**Figure 12.** Impacts of ENSO and tropical North Atlantic SSTs on Sep-Nov surface-climate across the continental U.S. The columns represent (left column) Standardized Precipitation Index (SPI) and MERRA-2 vertically integrated moisture transports, (middle column) reference evapotranspiration (ETo), and (right column) soil drying. The top two rows indicate how each of these three variables correlated with the atmospheric component of ENSO (ENSO P) and the Tropical North Atlantic (TNA) index, respectively, in 1980–2015. The third row shows estimates of (g) SPI and moisture transports, (h) ETo, and (i) soil drying for 2016 based on a multiple-linear regression with ENSO P and TNA for 1980–2015 (combined effects of ENSO P and TNA are referred to as "combo" in the figure). The bottom row shows the anomalies in 2016 that were not accounted for by the multiple regression with ENSO P and TNA. The green polygon bounds the SE U.S. study region.

Additionally, we see is no clear evidence for tropical teleconnections driving the low-frequency SE U.S. wetting trend observed over the course of the 20th century. If linked to a tropical teleconnection, 20th-century wetting would be expected to correspond to trends toward more El Niño-like SST patterns in the tropical Pacific and/or cooler SSTs in the tropical Atlantic, but this was not the case. Likewise, comparison between 1895 and 1956 (when 68% of fall seasons had below-average SE U.S. $SM_{MCDI}$) and 1957–2016 (when 45% of fall seasons had-below average SE U.S. $SM_{MCDI}$) indicates essentially no difference between the frequency of fall seasons experiencing La Niña conditions (negative Niño 3.4 SST anomaly), warm tropical Atlantic SSTs (positive TNA anomaly), or a combination of these two (1895–2016 SST data from Rayner et al., 2006).

## 4. Discussion

According to land-surface modeling over the relatively short period of 1979–2016, fall 2016 was exceptional in terms of soil dryness, rate of drying, and timing of peak dryness. Estimating soil moisture ($SM_{MCDI}$) back to 1895, we find several other periods, mostly concentrated in the first half of 1895–2016, when regionally averaged SE U.S. fall soil-moisture deficits were similar to those of 2016 and soil-moisture deficits in 1954 were likely more severe. In terms of duration and extent, the drought of 1953–1957 dwarfed the 2016 event and

tree-ring records indicate droughts in the middle of the last millennium that were far longer still (Seager et al., 2009). The centennial perspective presented in this paper highlights that extreme droughts like the 2016 event may be more likely than suggested by an evaluation that only considers the past 30–60 years. It is notable, however, that on the subregional scale, the fall 2016 drought may have still been the most severe on record across much of the southern Appalachians, where high forest-fire activity occurred. Further, the 2016 drought may have been particularly surprising because it was in stark contrast to significant trends over the past century toward wetter and cooler conditions in the SE U.S.

While the 2016 SE U.S. drought was primarily driven by a precipitation shortfall, an important secondary contributor was record-high atmospheric moisture demand during Sep-Nov, brought on by record-high daytime temperatures. This raises questions as to the potential contribution of anthropogenic radiative forcing to SE U.S. drought in 2016. Importantly, 20th-century cooling in the SE U.S., and indeed across much of the eastern U.S., was counter to the expected warming based on climate-model simulations. Possible contributors to cooling were midcentury increases in aerosol loading, low-frequency oscillations in the Pacific and North Atlantic basins, and enhanced evapotranspiration due to increased precipitation, forest cover, and irrigation (Baidya Roy et al., 2003; Chen et al., 2012; Ellenburg et al., 2016; Kunkel et al., 2006; Leibensperger et al., 2012a; Leibensperger et al., 2012b; Mascioli et al., 2017; Misra et al., 2012; Pan et al., 2004; Yu et al., 2014). However, the SE U.S. and much of the rest of the eastern U.S. has warmed since the 1970s, particularly at night, potentially signifying an emergence of projected trends, but also likely associated with multidecade variability in tropical Atlantic SSTs and reductions in aerosol load. While unresolved questions regarding the drivers of wetting and cooling in the SE U.S. preclude us from carrying out an attribution of anthropogenic forcing on drought intensity in 2016, the substantial secondary effect of record-high temperatures on drought in 2016 serves as an important reminder that extreme warmth can push a somewhat severe drought to record or near-record levels and promote the rapid development of so-called "flash drought" events (Hobbins et al., 2016; Wang et al., 2016).

Increased soil moisture during 1895–2015 was primarily driven by increasing precipitation, and this precipitation trend was largely driven by a nearly 50% increase in fall. The increase in fall precipitation may be in part related to general fall-wetting trends across much of the eastern U.S. For the Northeast U.S., the increase occurred as an as-yet undiagnosed wet shift following a drought in the 1960s (Seager et al., 2012). For the SE U.S., a wide range of factors are suggested to have contributed to the wetting trends, including decreased aerosol concentrations since the 1970s (Diem, 2013b; Leibensperger et al., 2012a; Westervelt et al., 2017), 20th-century reforestation (Baidya Roy et al., 2003; Chen et al., 2012), irrigation (Ozdogan et al., 2010; Puma & Cook, 2010), multidecadal oscillations in large-scale ocean and atmospheric circulation (McCabe et al., 2004; Meehl et al., 2012; Nigam et al., 2011; Wang et al., 2009), increased specific humidity due to greenhouse forcing (Diem, 2013a), changes in the position of the subtropical Atlantic high that may or may not be related to anthropogenic forcing (Diem, 2013a; Li et al., 2011; Li et al., 2012; Li et al., 2013), and internal atmospheric variability (Seager et al., 2012). Future work is needed to better understand the reasons for the increase in SE U.S. precipitation over the past century in order to guide expectations of precipitation trends in the coming decades.

In 2016, the primary cause of the precipitation shortfall was a suppression of southerly moisture transports into the SE U.S. from the Gulf of Mexico, caused by northerly wind anomalies throughout the atmospheric column over the eastern U.S. These northerly wind anomalies were driven largely by an anomalous ridge centered over the central U.S. that was, in part, promoted by hemispheric-scale circulation anomalies associated with both La Niña conditions and warm SSTs in the tropical and subtropical Atlantic. The teleconnection between fall drying in the SE U.S. and the cold Pacific/warm Atlantic combination is consistent in sign with observational and model results presented by many others, particularly for the winter half of the year (Gershunov & Cayan, 2003; Kurtzman & Scanlon, 2007; Kushnir et al., 2010; Mo & Schemm, 2008; Nigam et al., 2011; Ropelewski & Halpert, 1986; Ropelewski & Halpert, 1996; Seager et al., 2009; Tootle & Piechota, 2006; Wang et al., 2010; Wise et al., 2015; Wu et al., 2005). However, based on our correlation analysis, the tropical Pacific and Atlantic SST anomalies in 2016 were not strong enough to account for a sizable proportion of the extreme SE U.S. drying in fall 2016. This suggests that the atmospheric circulation anomalies that suppressed precipitation and enhanced evaporative demand in the SE U.S. in fall 2016 were primarily driven by internal atmospheric variability and only slightly amplified by teleconnections to the tropics. This result is consistent with prior findings that the teleconnection between the tropics and SE

U.S. hydroclimate is often overwhelmed by internal atmospheric variability (Seager et al., 2009). The dominant role of internal atmospheric variability was supported by the SST-forced CAM5.3 simulations that we evaluated.

Regarding the future, Earth System Models tend to project moderately negative trends in mean SE U.S. soil moisture over the 21st century (Berg et al., 2016; Cook et al., 2015). The projected reductions in mean SE U.S. soil moisture occur despite projected increases in mean annual precipitation and are likely driven by warming, decreased summer precipitation, and a trend toward heavier precipitation over fewer days, which may reduce infiltration (Berg et al., 2016; Polade et al., 2014). These model projections of future drying, our finding that warmth can substantially enhance drought severity in the SE U.S., and the existence of undiagnosed low-frequency precipitation variability in the historical record collectively motivate our conclusion that severe SE U.S. droughts will likely be more probable in the coming decades than would be suggested by an analysis of only the past 30–60 years.

We also note that there are important caveats to our conclusions. An aspect that complicates comparison of the 2016 drought to historical droughts is the major reforestation of the SE U.S., and indeed much of the eastern U.S., over the past century following massive deforestation during the 1600s through 1800s for agriculture and logging (Steyaert & Knox, 2008). Vegetation affects evapotranspiration and other surface processes such as above- and below-ground runoff. Throughout our study period of 1895–2016, we assume stationary surface resistance in the ETo calculation and a constant annual cycle in soil-moisture persistence derived from NLDAS2 data. In reality, changes in vegetation cover (Mankin et al., 2017; Nowacki & Abrams, 2008; Oudin et al., 2008), atmospheric carbon dioxide (Farquhar, 1997; Keller et al., 2017; Swann et al., 2016), nitrogen deposition (Magnani et al., 2007), ozone pollution (Felzer et al., 2004), rain acidity (Driscoll et al., 2001), urban cover (Scalenghe & Marsan, 2009), and interactions among these factors (e.g., Reich et al., 2006) affect how a given climatological event affects soil moisture via their influences on evapotranspiration. How these factors combined to affect soil moisture in 2016 is a complex question worthy of future research involving coupled Earth System Models and interpretations of their representation of the plant hydraulic response to changes in biogeochemistry and resultant land-atmosphere feedbacks (Quillet et al., 2010). Currently, LSM simulations of historical soil-moisture variability (e.g., Livneh & Hoerling, 2016; Mao et al., 2015; Shukla et al., 2015), including those done through the NLDAS2, do not account for how changes in land-surface characteristics or atmospheric chemistry would have modulated the effects of precipitation and ETo anomalies on soil moisture.

## 5. Conclusions

Our analysis of climatologically driven changes in SE U.S. soil moisture and the dynamical processes that drive these changes indicates that the climatological drought in the fall of 2016 was the most severe on record during the short period of 1979–2016 during which LSMs are used for operational monitoring. Expanding to a longer perspective from 1895 to present, however, indicates that several droughts of comparable magnitude have occurred over that time span, including a far longer and more spatially extensive drought from 1953 to 1957. The clustering of strong fall drought events between 1895 and 1956, and a dearth of similar events between 1957 and 2015, was due to an as-yet undiagnosed shift in the SE U.S. toward increased precipitation, particularly in fall, and decreased daytime temperatures. Record-high temperatures in fall 2016 aided the intensification of the drought by producing record-high levels of atmospheric moisture demand.

The drought in the fall of 2016 may have been partly promoted by La Niña-like conditions in the tropical Pacific and warm conditions in the tropical Atlantic that combined to limit moisture transports and promote warmth in the SE U.S., but these tropical anomalies were not strong enough in fall 2016 to account for the extreme hydroclimate anomalies observed in the SE U.S. The majority of the extreme SE U.S. soil drying that occurred in fall 2016 therefore appears to have arisen as a result of internal atmospheric variability, with only a small additional influence, if at all, from tropical teleconnections.

While extreme drought has been rare in the SE U.S. over the past half century, the intensity and rapid onset of the SE U.S. drought in 2016, and its destructive impacts on wildfire and human water resources, should motivate preparedness for reoccurrences of droughts of similar or stronger magnitude, particularly in light of model projections of future warming and reduced soil moisture as well as tree-ring evidence

that attests to much longer SE U.S. droughts in the middle of the last millennium. The 2016 SE U.S. drought also provides motivation to better understand the causes of the significant increase in SE U.S. precipitation over the past century and what the fate of this trend will be in the coming decades.

**Acknowledgments**
We provide gridded 1/8° soil-moisture and climate datasets for the continental U.S. online at http://www.ldeo.columbia.edu/~williams/se_drought_2017_jgr.html. The climate and modeled soil-moisture data sets accessed for this study are publicly available, and the sources are listed in Table S1. Thanks to Dong-Eun Lee of LDEO for generating the CAM5.3 ensemble. Williams was supported by the National Science Foundation (NSF) grant AGS-1703029 and the Center for Climate and Life at Columbia University. Williams, Cook, and Seager were supported in part by the NASA Modeling, Analysis, and Prediction program (16-MAP16-0081). Bishop was supported by a NASA Earth and Space Science Graduate Student Fellowship (17-EARTH17F-0038). Smerdon and Seager were supported in part by NSF AGS-1401400. Mankin was supported in part by a Columbia University Earth Institute Postdoctoral Fellowship. Lamont contribution 8147.

## References

Adler, R. F., Huffman, G. J., Chang, A., Ferraro, R., Xie, P.-P., Janowiak, J., … Nelkin, E. (2003). The version-2 Global Precipitation Climatology Project (GPCP) monthly precipitation analysis (1979–present). *Journal of Hydrometeorology*, *4*(6), 1147–1167. https://doi.org/10.1175/1525-7541(2003)004%3C1147:TVGPCP%3E2.0.CO;2

Ahillen, S. (2016). A month after historic fire, Gatlinburg rebuilds, Knoxville News Sentinel, Knoxville, TN, December 28 2016. http://www.knoxnews.com/story/news/local/tennessee/2016/12/28/month-after-historic-fire-gatlinburg-rebuilding/95754104/.

Allen, R. G., Pereira L. S., Raes D., & Smith M. (1998). Crop evapotranspiration—Guidelines for computing crop water requirements-FAO Irrigation and drainage, paper 56, 15 pp, Food and Agriculture Organizatoin of the United Nations, Rome. http://www.fao.org/docrep/x0490e/x0490e07.htm-radiation

Baidya Roy, S., Hurtt, G. C., Weaver, C. P., & Pacala, S. W. (2003). Impact of historical land cover change on the July climate of the United States. *Journal of Geophysical Research: Atmospheres*, *108*(D24), 4793. https://doi.org/10.1029/2003JD003565

Berg, A., Sheffield, J., & Milly, P. C. D. (2016). Divergent surface and total soil moisture projections under global warming. *Geophysical Research Letters*, *44*(1), 236–244. https://doi.org/10.1002/2016GL071921

Chen, G., Tian, H., Zhang, C., Liu, M., Ren, W., Zhu, W., … Lockaby, G. B. (2012). Drought in the Southern United States over the 20th century: Variability and its impacts on terrestrial ecosystem productivity and carbon storage. *Climatic Change*, *114*(2), 379–397. https://doi.org/10.1007/s10584-012-0410-z

Chen, G.-S., Notaro, M., Liu, Z., & Liu, Y. (2012). Simulated local and remote biophysical effects of afforestation over the southeast United States in boreal summer. *Journal of Climate*, *25*(13), 4511–4522. https://doi.org/10.1175/JCLI-D-11-00317.1

Compo, G. P., Whitaker, J. S., Sardeshmukh, P. D., Matsui, N., Allan, R. J., Yin, X., … Worley, S. J. (2011). The Twentieth Century Reanalysis project. *Quarterly Journal of the Royal Meteorological Society*, *137*(654), 1–28. https://doi.org/10.1002/qj.776

Cook, B. I., Ault, T. R., & Smerdon, J. E. (2015). Unprecedented 21st century drought risk in the American Southwest and Central Plains. *Science Advances*, *1*(1), e1400082. https://doi.org/10.1126/sciadv.1400082

Cook, B. I., Smerdon, J. E., Seager, R., & Coats, S. (2014). Global warming and 21st century drying. *Climate Dynamics*, *43*(9–10), 2607–2627. https://doi.org/10.1007/s00382-014-2075-y

Cook, E. R., Kablack, M. A., & Jacoby, G. C. (1988). The 1986 drought in the southeastern United States: How rare an event was it? *Journal of Geophysical Research: Atmospheres*, *93*(D11), 14,257–14,260. https://doi.org/10.1029/JD093iD11p14257

Dai, A., Lin, X., & Hsu, K.-L. (2007). The frequency, intensity, and diurnal cycle of precipitation in surface and satellite observations over low- and mid-latitudes. *Climate Dynamics*, *29*(7–8), 727–744. https://doi.org/10.1007/s00382-007-0260-y

Daly, C., Halbleib, M., Smith, J. I., Gibson, W. P., Doggett, M. K., Taylor, G. H., … Pasteris, P. P. (2008). Physiographically sensitive mapping of climatological temperature and precipitation across the conterminous United States. *International Journal of Climatology*, *28*(15), 2031–2064. https://doi.org/10.1002/joc.1688

Diem, J. E. (2013a). Influences of the Bermuda High and atmospheric moistening on changes in summer rainfall in the Atlanta, Georgia region, USA. *International Journal of Climatology*, *33*(1), 160–172. https://doi.org/10.1002/joc.3421

Diem, J. E. (2013b). The 1970 Clean Air Act and termination of rainfall suppression in a U.S. urban area. *Atmospheric Environment*, *75*, 141–146. https://doi.org/10.1016/j.atmosenv.2013.04.041

Driscoll, C. T., Lawrence, G. B., Bulger, A. J., Butler, T. J., Cronan, C. S., Eagar, C., … Weathers, K. C. (2001). Acidic deposition in the Northeastern United States: Sources and inputs, ecosystem effects, and management strategies: The effects of acidic deposition in the northeastern United States include the acidification of soil and water, which stresses terrestrial and aquatic biota. *Bioscience*, *51*(3), 180–198. https://doi.org/10.1641/0006-3568(2001)051%5B0180:ADITNU%5D2.0.CO;2

Eidenshink, J., Schwind, B., Brewer, K., Zhu, Z., Quayle, B., & Howard, S. (2007). A project for monitoring trends in burn severity. *Fire Ecology*, *3*(1), 3–21. https://doi.org/10.4996/fireecology.0301003

Ek, M. B., Mitchell, K. E., Lin, Y., Rogers, E., Grunmann, P., Koren, V., … Tarpley, J. D. (2003). Implementation of Noah land surface model advances in the National Centers of Environmental operation mesoscale Eta model. *Journal of Geophysical Research*, *108*, 8851. https://doi.org/10.1029/2002JD003296

Ellenburg, W. L., McNider, R. T., Cruise, J. F., & Christy, J. R. (2016). Towards an understanding of the twentieth-century cooling trend in the Southeastern United States: Biogeophysical impacts of land-use change. *Earth Interactions*, *20*(18), 1–31. https://doi.org/10.1175/EI-D-15-0038.1

Enfield, D. B., Mestas-Nuñez, A. M., Mayer, D. A., & Cid-Serrano, L. (1999). How ubiquitous is the dipole relationship in tropical Atlantic sea surface temperatures? *Journal of Geophysical Research: Oceans*, *104*(C4), 7841–7848. https://doi.org/10.1029/1998JC900109

Farquhar, G. D. (1997). Carbon dioxide and vegetation. *Science*, *278*(5342), 1411. https://doi.org/10.1126/science.278.5342.1411

Felzer, B., Kicklighter, D., Melillo, J., Wang, C., Zhuang, Q., & Prinn, R. (2004). Effects of ozone on net primary production and carbon sequestration in the conterminous United States using a biogeochemistry model. *Tellus B*, *56*(3), 230–248. https://doi.org/10.1111/j.1600-0889.2004.00097.x

Gershunov, A., & Barnett, T. P. (1998). Interdecadal modulation of ENSO teleconnections. *Bulletin of the American Meteorological Society*, *79*(12), 2715–2725. https://doi.org/10.1175/1520-0477(1998)079%3C2715:IMOET%3E2.0.CO;2

Gershunov, A., & Cayan, D. R. (2003). Heavy daily precipitation frequency over the contiguous United States: Sources of climatic variability and seasonal predictability. *Journal of Climate*, *16*(16), 2752–2765. https://doi.org/10.1175/1520-0442(2003)016%3C2752:HDPFOT%3E2.0.CO;2

Harris, I., Jones, P. D., Osborn, T. J., & Lister, D. H. (2014). Updated high-resolution grids of monthly climatic observations—The CRU TS3.10. *Dataset, International Journal of Climatology*, *34*(3), 623–642. https://doi.org/10.1002/joc.3711

Higgins, R. W., Leetmaa, A., Xue, Y., & Barnston, A. (2000). Dominant factors influencing the seasonal predictability of U.S. precipitation and surface air temperature. *Journal of Climate*, *13*(22), 3994–4017. https://doi.org/10.1175/1520-0442(2000)013%3C3994:DFITSP%3E2.0.CO;2

Hobbins, M., Wood, A., McEvoy, D., Huntington, J., Morton, C., Verdin, J., … Hain, C. (2016). The Evaporative Demand Drought Index: Part I—Linking drought evolution to variations in evaporative demand. *Journal of Hydrometeorology*, *17*(6), 1745–1761. https://doi.org/10.1175/JHM-D-15-0121.1

Keller, K. M., Lienert, S., Bozbiyik, A., Stocker, T. F., Churakova, O. V. (Sidorova), Frank, D. C., … Joos, F. (2017). 20th century changes in carbon isotopes and water-use efficiency: Tree-ring-based evaluation of the CLM4.5 and LPX-Bern models. *Biogeosciences*, *14*(10), 2641–2673. https://doi.org/10.5194/bg-14-2641-2017

Klos, R. J., Wang, G. G., Bauerle, W. L., & Rieck, J. R. (2009). Drought impact on forest growth and mortality in the southeast USA: An analysis using Forest Health and Monitoring data. *Ecological Applications*, *19*(3), 699–708. https://doi.org/10.1890/08-0330.1

Koster, R. D., & Suarez, M. J. (1994). The components of a 'SVAT' scheme and their effects on a GCM's hydrological cycle. *Advances in Water Resources*, *17*(1), 61–78. https://doi.org/10.1016/0309-1708(94)90024-8

Koster, R. D., Wang, H., Schubert, S. D., Suarez, M. J., & Mahanama, S. (2009). Drought-induced warming in the continental United States under different SST regimes. *Journal of Climate*, *22*(20), 5385–5400. https://doi.org/10.1175/2009JCLI3075.1

Kunkel, K. E., Liang, X.-Z., Zhu, J., & Lin, Y. (2006). Can CGCMs simulate the twentieth-century "warming hole" in the central United States? *Journal of Climate*, *19*(17), 4137–4153. https://doi.org/10.1175/JCLI3848.1

Kurtzman, D., & Scanlon, B. R. (2007). El Nino–Southern Oscillation and Pacific Decadal Oscillation impacts on precipitation in the southern and central United States: Evaluation of spatial distribution and predictions. *Water Resources Research*, *43*, W10527. https://doi.org/10.1029/2007WR005863

Kushnir, Y., Seager, R., Ting, M., Naik, N., & Nakamura, J. (2010). Mechanisms of tropical Atlantic SST influence on North American precipitation variability. *Journal of Climate*, *23*(21), 5610–5628. https://doi.org/10.1175/2010JCLI3172.1

Leibensperger, E. M., Mickley, L. J., Jacob, D. J., Chen, W.-T., Seinfeld, J. H., Nenes, A., … Rind, D. (2012a). Climatic effects of 1950–2050 changes in U.S. anthropogenic aerosols—Part 2: Climate response. *Atmospheric Chemistry and Physics*, *12*(7), 3349–3362. https://doi.org/10.5194/acp-12-3349-2012

Leibensperger, E. M., Mickley, L. J., Jacob, D. J., Chen, W.-T., Seinfeld, J. H., Nenes, A., … Rind, D. (2012b). Climatic effects of 1950–2050 changes in U.S. anthropogenic aerosols—Part 1: Aerosol trends and radiative forcing. *Atmospheric Chemistry and Physics*, *12*(7), 3333–3348. https://doi.org/10.5194/acp-12-3333-2012

Li, L., Li, W., & Deng, Y. (2013). Summer rainfall variability over the Southeastern United States and its intensification in the 21st century as assessed by CMIP5 models. *Journal of Geophysical Research: Atmospheres*, *118*(2), 340–354. https://doi.org/10.1002/jgrd.50136

Li, W., Li, L., Fu, R., Deng, Y., & Wang, H. (2011). Changes to the North Atlantic subtropical high and its role in the intensification of summer rainfall variability in the southeastern United States. *Journal of Climate*, *24*(5), 1499–1506. https://doi.org/10.1175/2010JCLI3829.1

Li, W., Li, L., Ting, M., & Liu, Y. (2012). Intensification of Northern Hemisphere subtropical highs in a warming climate. *Nature Geoscience*, *5*(11), 830–834. https://doi.org/10.1038/ngeo1590

Livneh, B., & Hoerling, M. P. (2016). The physics of drought in the U.S. Central Great Plains. *Journal of Climate*, *29*, 6783–6804. https://doi.org/10.1175/JCLI-D-15-0697.1

Magnani, F., Mencuccini, M., Borghetti, M., Berbigier, P., Berninger, F., Delzon, S., … Grace, J. (2007). The human footprint in the carbon cycle of temperate and boreal forests. *Nature*, *447*(7146), 849–851. https://doi.org/10.1038/nature05847

Mankin, J. S., Smerdon, J. E., Cook, B. I., Williams, A. P., & Seager, R. (2017). The curious case of projected 21st-century drying but greening in the American West. *Journal of Climate*, *30*(21), 8689–8710. https://doi.org/10.1175/JCLI-D-17-0213.1

Mao, Y., Nijssen, B., & Lettenmaier, D. P. (2015). Is climate change implicated in the 2013–2014 California drought? A hydrologic perspective. *Geophysical Research Letters*, *42*(8), 2805–2813. https://doi.org/10.1002/2015GL063456

Mascioli, N. R., Previdi, M., Fiore, A. M., & Ting, M. (2017). Timing and seasonality of the United States 'warming hole'. *Environmental Research Letters*, *12*(3). 034008. https://doi.org/10.1088/1748-9326/aa5ef4

McCabe, G. J., Palecki, M. A., & Betancourt, J. L. (2004). Pacific and Atlantic Ocean influences on multidecadal drought frequency in the United States. *Proceedings of the National Academy of Sciences USA*, *101*(12), 4136–4141. https://doi.org/10.1073/pnas.0306738101

Meehl, G. A., Arblaster, J. M., & Branstator, G. (2012). Mechanisms contributing to the warming hole and the consequent U.S. east-west differential of heat extremes. *Journal of Climate*, *25*(18), 6394–6408. https://doi.org/10.1175/JCLI-D-11-00655.1

Michaelsen, J. (1987). Cross-validation in statistical climate forecast models. *Journal of Applied Meteorology*, *26*(11), 1589–1600. https://doi.org/10.1175/1520-0450(1987)026%3C1589:CVISCF%3E2.0.CO;2

Misra, V., Michael, J.-P., Boyles, R., Chassignet, E. P., Griffin, M., & O'Brien, J. J. (2012). Reconciling the spatial distribution of the surface temperature trends in the southeastern United States. *Journal of Climate*, *25*(10), 3610–3618. https://doi.org/10.1175/JCLI-D-11-00170.1

Mo, K. C., & Schemm, J. E. (2008). Relationships between ENSO and drought over the southeastern United States. *Geophysical Research Letters*, *35*, L15701. https://doi.org/10.1029/2008GL034656

Molod, A., Takacs, L., Suarez, M., & Bacmeister, J. (2015). Development of the GEOS-5 atmospheric general circulation model: Evolution from MERRA to MERRA2. *Geoscientific Model Development*, *8*(5), 1339–1356. https://doi.org/10.5194/gmd-8-1339-2015

Monteith, J. L. (1965). Evaporation and environment, Symoposia of the Society for Experimental Biology, 19, 205–234. http://www.unc.edu/courses/2007fall/geog/801/001/www/ET/Monteith65.pdf.

NASA (2016). Drought and fire in the southeast, Earth Observatory, National Aeronautics and Space Agency, Washington, D.C., November 11 2016. https://earthobservatory.nasa.gov/IOTD/view.php?id=89103

Nigam, S., Guan, B., & Ruiz-Barradas, A. (2011). Key role of the Atlantic Multidecadal Oscillation in 20th century drought and wet periods over the Great Plains. *Geophysical Research Letters*, *38*, L16713. https://doi.org/10.1029/2011GL048650

Niu, G.-Y., Yang, Z.-L., Mitchell, K. E., Chen, F., Ek, M. B., Barlage, M., … Xia, Y. (2011). The community Noah land surface model with multi-parameterization options (Noah-MP): 1. Model description and evaluation with local-scale measurements. *Journal of Geophysical Research Atmospheres*, *116*(D12), D12109. https://doi.org/10.1029/2010JD015139

Nowacki, G. J., & Abrams, M. D. (2008). The demise of fire and "mesophication" of forests in the eastern United States. *Bioscience*, *58*(2), 123–138. https://doi.org/10.1641/B580207

Oudin, L., Andréassian, V., Lerat, J., & Michel, C. (2008). Has land cover a significant impact on mean annual streamflow? An international assessment using 1508 catchments. *Journal of Hydrology*, *357*(3), 303–316. https://doi.org/10.1016/j.jhydrol.2008.05.021

Oyler, J. W., Ballantyne, A., Jencso, K., Sweet, M., & Running, S. W. (2015). Creating a topoclimatic daily air temperature dataset for the conterminous United States using homogenized station data and remotely sensed land skin temperature. *International Journal of Climatology*, *35*(9), 2258–2279. https://doi.org/10.1002/joc.4127

Ozdogan, M., Rodell, M., Beaudoing, H. K., & Toll, D. L. (2010). Simulating the effects of irrigation over the United States in a land surface model based on satellite-derived agricultural data. *Journal of Hydrometeorology*, *11*(1), 171–184. https://doi.org/10.1175/2009JHM1116.1

Palmer, W. C. (1965). Meteorological drought, 58 pp, United States Weather Bureau, Washington, DC. https://docs.lib.noaa.gov/rescue/wb_researchpapers/QC852U55no45.pdf

Pan, Z., Arritt, R. W., Takle, E. S., Gutowski, W. J., Anderson, C. J., & Segal, M. (2004). Altered hydrologic feedback in a warming climate introduces a "warming hole". *Geophysical Research Letters*, *31*, L17109. https://doi.org/10.1029/2004GL020528

Polade, S. D., Pierce, D. W., Cayan, D. R., Gershunov, A., & Dettinger, M. D. (2014). The key role of dry days in changing regional climate and precipitation regimes. *Scientific Reports*, *4*, 4364. https://doi.org/10.1038/srep04364

Puma, M. J., & Cook, B. I. (2010). Effects of irrigation on global climate during the 20th century. *Journal of Geophysical Research*, *115*, D16120. https://doi.org/10.1029/2010JD014122

Quillet, A., Peng, C., & Garneau, M. (2010). Toward dynamic global vegetation models for simulating vegetation-climate interactions and feedbacks: Recent developments, limitations, and future challenges. *Environmental Reviews*, *18*(NA), 333–353. https://doi.org/10.1139/A10-016

Rayner, N. A., Brohan, P., Parker, D. E., Folland, C. K., Kennedy, J. J., Vanicek, M., … Tett, S. F. B. (2006). Improved analyses of changes and uncertainties in sea surface temperature measured in situ since the mid-nineteenth century: The HadSST2 dataset. *Journal of Climate*, *19*(3), 446–469. https://doi.org/10.1175/JCLI3637.1

Reich, P. B., Hobbie, S. E., Lee, T., Ellsworth, D. S., West, J. B., Tilman, D., … Trost, J. (2006). Nitrogen limitation constrains sustainability of ecosystem response to $CO_2$. *Nature*, *440*(7086), 922–925. https://doi.org/10.1038/nature04486

Rienecker, N. M., Suarez, M. J., Gelaro, R., Todling, R., Bacmeister, J., Liu, E., … Woollen, J. (2011). MERRA-NASA's Modern-Era Retrospective Analysis for Research and Applications. *Journal of Climate*, *24*(14), 3624–3648. https://doi.org/10.1175/jcli-d-11-00015.1

Rodell, M., Houser, P. R., Jambor, U., Gottschalck, J., Mitchell, K., Meng, C. J., … Bosilovich, M. (2004). The global land data assimilation system. *Bulletin of the American Meteorological Society*, *85*(3), 381–394. https://doi.org/10.1175/BAMS-85-3-381

Rohde, R., Muller, R. A., Jacobsen, R., Muller, E., Perlmutter, S., Rosenfeld, A., … Wickham, C. (2013). A new estimate of the average Earth surface land temperature spanning 1753 to 2011. *Geoinformatics & Geostatistics: An Overview*, *1*(1), 1–7. https://doi.org/10.4172/2327-4581.1000101

Ropelewski, C., & Halpert, M. (1986). North American precipitation and temperature patterns associated with the El Niño/Southern Oscillation (ENSO). *Monthly Weather Review*, *114*(12), 2352–2362. https://doi.org/10.1175/1520-0493%281986%29114%3C2352%3ANAPATP%3E2.0.CO%3B2

Ropelewski, C. F., & Halpert, M. S. (1996). Quantifying Southern Oscillation-precipitation relationships. *Journal of Climate*, *9*, 1043–1059. https://doi.org/10.1175/1520-0442(1996)009%3C1043:QSOPR%3E2.0.CO;2

Roy, D. P., Boschetti, L., Justice, C. O., & Ju, J. (2008). The Collection 5 MODIS burned area product—Global evaluation by comparison with the MODIS active fire product. *Remote Sensing of Environment*, *112*(9), 3690–3707. https://doi.org/10.1016/j.rse.2008.05.013

Samuel, M. (2016). Florida and Georgia argue in court over water rights, All Things Considered, National Public Radio, Washington, D.C., October 30 2016. http://www.npr.org/2016/10/30/499985890/florida-and-georgia-argue-in-court-over-water-rights

Scalenghe, R., & Marsan, F. A. (2009). The anthropogenic sealing of soils in urban areas. *Landscape and Urban Planning*, *90*(1), 1–10. https://doi.org/10.1016/j.landurbplan.2008.10.011

Schneider, U., Becker, A., Finger, P., Meyer-Christoffer, A., Ziese, M., & Rudolf, B. (2014). GPCC's new land surface precipitation climatology based on quality-controlled in situ data and its role in quantifying the global water cycle. *Theoretical and Applied Climatology*, *115*(1–2), 15–40. https://doi.org/10.1007/s00704-013-0860-x

Seager, R., Goddard, L., Nakamura, J., Henerson, N., & Lee, D. E. (2014). Dynamical causes of the 2010/11 Texas-northern Mexico drought. *Journal of Hydrometeorology*, *15*, 39–68. https://doi.org/10.1175/JHM-D-13-024.1

Seager, R., Pederson, N., Kushnir, Y., Nakamura, J., & Jurburg, S. (2012). The 1960s drought and the subsequent shift to a wetter climate in the Catskill Mountains Region of the New York City Watershed. *Journal of Climate*, *25*(19), 6721–6742. https://doi.org/10.1175/JCLI-D-11-00518.1

Seager, R., Tzanova, A., & Nakamura, J. (2009). Drought in the southeastern United States: Causes, variability over the last millennium, and the potential for future hydroclimate change. *Journal of Climate*, *22*(19), 5021–5045. https://doi.org/10.1175/2009JCLI2683.1

Sen, P. B. (1968). Estimates of the regression coefficient based on Kendall's Tau. *Journal of the American Statistical Association*, *63*(324), 1379–1389.

Seneviratne, S. I., Corti, T., Davin, E. L., Hirschi, M., Jaeger, E. B., Lehner, I., … Teuling, A. J. (2010). Investigating soil moisture-climate interactions in a changing climate: A review. *Earth-Science Reviews*, *99*(3), 125–161. https://doi.org/10.1016/j.earscirev.2010.02.004

Sheffield, J., Goteti, G., & Wood, E. F. (2006). Development of a 50-yr high-resolution global dataset of meteorological forcings for land surface modeling. *Journal of Climate*, *19*(13), 3088–3111. https://doi.org/10.1175/JCLI3790.1

Shukla, S., Safeeq, M., AghaKouchak, A., Guan, K., & Funk, C. (2015). Temperature impacts on the water year 2014 drought in California. *Geophysical Research Letters*, *42*(11), 4384–4393. https://doi.org/10.1002/2015GL063666

Steinemann, A. (2014). Drought information for improving preparedness in the western states. *Bulletin of the American Meteorological Society*, *95*(6), 843–847. https://doi.org/10.1175/BAMS-D-13-00067.1

Steinemann, A., Iacobellis, S. F., & Cayan, D. R. (2015). Developing and evaluating drought indicators for decision-making. *Journal of Hydrometeorology*, *16*(4), 1793–1803. https://doi.org/10.1175/JHM-D-14-0234.1

Steyaert, L. T., & Knox, R. G. (2008). Reconstructed historical land cover and biophysical parameters for studies of land-atmosphere interactions within the eastern United States. *Journal of Geophysical Research: Atmospheres*, *113*, D02101. https://doi.org/10.1029/2006JD008277

Svoboda, M., LeComte, D., Hayes, M., Heim, R., Gleason, K., Angel, J., … Stephens, S. (2002). The Drought Monitor. *Bulletin of the American Meteorological Society*, *83*(8), 1181–1190. https://doi.org/10.1175/1520-0477%282002%29083%3C1181:TDM%3E2.3.CO;2

Swann, A. L. S., Hoffman, F. M., Koven, C. D., & Randerson, J. T. (2016). Plant responses to increasing $CO_2$ reduce estimates of climate impacts on drought severity. *Proceedings of the National Academy of Sciences USA*, *113*(36), 10,019–10,024. https://doi.org/10.1073/pnas.1604581113

Ting, M., Kushnir, Y., & Li, C. (2014). North Atlantic multidecadal SST oscillation: External forcing versus internal variability. *Journal of Marine Systems*, *133*, 27–38. https://doi.org/10.1016/j.jmarsys.2013.07.006

Tootle, G. A., & Piechota, T. C. (2006). Relationships between Pacific and Atlantic Ocean sea surface temperatures and U.S. streamflow variability. *Water Resources Research*, *42*, W07411. https://doi.org/10.1029/2005WR004184

Trenberth, K. E., Branstator, G. W., & Arkin, P. A. (1988). Origins of the 1988 North American drought. *Science*, *242*(4886), 1640–1645. https://doi.org/10.1126/science.242.4886.1640

USDA (2017a). Crop values 2016 summary, Rep. 1949–0372, 14–16 pp, United States Department of Agriculture National Agricultural Statistics Service, Washington, D.C. http://usda.mannlib.cornell.edu/usda/current/CropValuSu/CropValuSu-02-24-2017_revision.pdf

USDA (2017b). Crop progress and conditions, United States Department of Agriculture National Agricultural Statistics Service, Washington, D.C. https%3A%2F%2Fwww.nass.usda.gov%2FCharts_and_Maps%2FCrop_Progress_%26_Condition%2F2017%2F

Vicente-Serrano, S. M., Begueria, S., & Lopez-Moreno, J. I. (2010). A multiscalar drought index sensitive to global warming: The standardized precipitation evapotranspiration index. *Journal of Climate*, *23*(7), 1696–1718. https://doi.org/10.1175/2009JCLI2909.1

Vose, R. S., Applequist, S., Squires, M., Durre, I., Menne, M. J., Williams, C. N. Jr., … Arndt, D. (2014). Improved historical temperature and precipitation time series for U.S. climate divisions. *Journal of Applied Meteorology and Climatology*, *53*(5), 1232–1251. https://doi.org/10.1175/JAMC-D-13-0248.1

Wang, H., Schubert, S., Suarez, M., Chen, J., Hoerling, M., Kumar, A., & Pegion, P. (2009). Attribution of the seasonality and regionality in climate trends over the United States during 1950–2000. *Journal of Climate*, *22*(10), 2571–2590. https://doi.org/10.1175/2008JCLI2359.1

Wang, H., Schubert, S., Suarez, M., & Koster, R. (2010). The physical mechanisms by which the leading patterns of SST variability impact U.S. precipitation. *Journal of Climate*, *23*(7), 1815–1836. https://doi.org/10.1175/2009JCLI3188.1

Wang, K. J., Williams, A. P., & Lettenmaier, D. P. (2017). How much have California winters warmed over the last century? *Geophysical Research Letters*, *44*, 8893–8900. https://doi.org/10.1002/2017GL075002

Wang, L., Yuan, X., Xie, Z., Wu, P., & Li, Y. (2016). Increasing flash droughts over China during the recent global warming hiatus. *Scientific Reports*, *6*, 30,571. https://doi.org/10.1038/srep30571

Westervelt, D. M., Conley, A. J., Fiore, A. M., Lamarque, J. F., Shindell, D., Previdi, M., … Horowitz, L. W. (2017). Multimodel precipitation responses to removal of U.S. sulfur dioxide emissions. *Journal of Geophysical Research: Atmospheres*, *122*(9), 5024–5038. https://doi.org/10.1002/2017JD026756

Williams, A. P., Seager, R., Abatzoglou, J. T., Cook, B. I., Smerdon, J. E., & Cook, E. R. (2015). Contribution of anthropogenic warming to California drought during 2012–2014. *Geophysical Research Letters*, *42*(16), 6819–6828. https://doi.org/10.1002/2015GL064924

Wise, E. K., Wrzesien, M. L., Dannenberg, M. P., & McGinnis, D. L. (2015). Cool-season precipitation patterns associated with teleconnection interactions in the United States. *Journal of Applied Meteorology and Climatology*, *54*(2), 494–505. https://doi.org/10.1175/JAMC-D-14-0040.1

Wood, E. F., Lettenmaier, D. P., & Zartarian, V. G. (1992). A land-surface hydrology parameterization with subgrid variability for general circulation models. *Journal of Geophysical Research: Atmospheres*, *97*(D3), 2717–2728. https://doi.org/10.1029/91JD01786

Wu, A., Hseih, W. W., & Shabbar, A. (2005). The nonlinear patterns of North American winter temperature and precipitation associated with ENSO. *Journal of Climate*, *18*, 1736–1752. https://doi.org/10.1175/JCLI3372.1

Xia, Y., Mitchell, K., Ek, M., Sheffield, J., Cosgrove, B., Wood, E., … Mocko, D. (2012a). Continental-scale water and energy flux analysis and validation for the North American Land Data Assimilation System project phase 2 (NLDAS-2): 1. Intercomparison and application of model products. *Journal of Geophysical Research: Atmospheres*, *117*, D03109. https://doi.org/10.1029/2011JD016051

Xia, Y., Mitchell, K., Ek, M., Sheffield, J., Cosgrove, B., Wood, E., … Mocko, D. (2012b). Continental-scale water and energy flux analysis and validation for North American Land Data Assimilation System project phase 2 (NLDAS-2): 2. Validation of model-simulated streamflow. *Journal of Geophysical Research: Atmospheres*, *117*, D03110. https://doi.org/10.1029/2011JD016051

Yin, D., Roderick, M. L., Leech, G., Sun, F., & Huang, Y. (2014). The contribution of reduction in evaporative cooling to higher surface air temperatures during drought. *Geophysical Research Letters*, *41*, 7891–7897. https://doi.org/10.1002/2014GL062039

Yu, S., Alapaty, K., Mathur, R., Pleim, J., Zhang, Y., Nolte, C., … Nagashima, T. (2014). Attribution of the United States "warming hole": Aerosol indirect effect and precipitable water vapor. *Scientific Reports*, *4*, 6929. https://doi.org/10.1038/srep06929